Static properties of classical Josephson junction arrays: models and experimental achievements

1999 J. Phys.: Condens. Matter 11 R361

(http://iopscience.iop.org/0953-8984/11/36/201)

J. Phys.: Condens. Matter **11** (1999) R361–R390. Printed in the UK PII: S0953-8984(99)90102-9

REVIEW ARTICLE

Static properties of classical Josephson junction arrays: models and experimental achievements

José C Ciria† and C Giovannella†‡

† Departamento de Fisica Teórica, Universidad de Zaragoza, C/Pedro Cerbuna 12, 50010 Zaragoza, Spain

‡ Dipartimento di Fisica, Sezione INFN and Sezione INFM dell'Università di Roma, Tor Vergata, Via della Ricerca Scientifica 1, 00133 Roma, Italy

Received 7 May 1999

Abstract. This review deals with the static properties of classical Josephson arrays. We first comment on the model describing the system, both in the phase representation—*the frustrated XY model*—and in the vortex representation—*the Coulomb gas model*. Self-induced magnetic fields and disorder are added so as to faithfully reproduce physical systems. A review of scaling theory concerning the I–V curve—which provides relevant information about, for example, the proximity of a phase transition—is given in order to compare theoretical predictions with experimental results. Josephson arrays are characterized by an extremely rich phase diagram as a function of both external parameters (temperature, applied magnetic field) and inherent ones (disorder, self-inductance). Such a diagram is explored in the light of recent results. Questions such as those of the nature of the ground state and the stability of the static states, and the existence of a disordered vortex state due to disorder intrinsic to the array and/or to external influences arise.

1. Introduction

Arrays of classical Josephson junctions (JJAs)—i.e. arrays where quantum effects are negligible—have been the object of an intense research effort in the last few years. The study of their properties is prompted by a wide range of stimuli. Many different areas of interest converge in this field: many-body problems, complex frustrated and/or disordered systems—exhibiting turbulence, chaos transitions etc—critical phenomena etc. Their possible technological applications as components of cryoelectronic devices are also relevant [1, 2].

Classical Josephson arrays are described in terms of 2π-periodic variables defined at the lattice sites (θ_i), whose instantaneous values (i.e. orientations) depend strongly on the interaction of the site with its nearest-neighbour ones. θ_i is the phase of the superconducting wave function of island i. They are isomorphic to an ensemble of spins free to rotate in the X–Y plane. Frustration is introduced in the model through variables defined at the links (a_{ij}, related to the potential vector of the magnetic field). An appropriate choice of gauge allows one to identify θ_i and a_{ij} with irrotational and solenoidal fields, respectively. An alternative description of the system is based on gauge-invariant variables $\phi_{ij} = \theta_i - \theta_j - a_{ij}$.

As a different approach, one may concentrate instead on the plaquette-like variables (vortices and antivortices, which correspond to quantized fluxoids), so that the system can be mapped onto the so-called Coulomb gas model.

Long-range coupling between the fields can be introduced (reflecting the physical fact of magnetic inductance). Furthermore, intrinsic and extrinsic perturbations can be implemented

0953-8984/99/360361+30$30.00

in a natural way (disordered geometry or local defects, applied magnetic fields, temperature fluctuations etc).

In this way, one can add more and more complexity to the initial system. All of these features find related counterparts in many different physical systems. Josephson arrays are physical realizations of the XY model where frustration, long-range interactions, disorder and external perturbations are naturally present; the ensemble of gauge-invariant phases can be straightforwardly mapped onto an array of coupled non-linear oscillators (admitting short- and long-range interactions); the description in terms of vortices/antivortices can be visualized as a system of interacting charges.

In nature there exist several realizations of planar spin systems or Coulomb gas systems, but many researchers preferred to focus their attention on the JJAs. This is because, thanks to the modern lithographic processes, it is possible to fabricate arrays with thousands of junctions whose parameters can be fixed with a high precision; the development of low-cost and powerful workstations and the improvement of more and more sophisticated experimental apparatus are other factors that contributed to the explosion of the subject. Reliable fabrication processes have been fundamental to control, i.e., the coupling strength, the amount and kind of disorder etc. Numerical simulations of the statical and dynamical properties of relatively large arrays are essential in order to interpret the measurements and, often, to suggest new experiments. Most numerical results would have been 'virtual reality' without the development of, for example, the very sensitive Bitter decoration and scanning SQUID or STM apparatuses that allow one to obtain 'WYSIWYG' pictures of the arrays and to confirm theoretical predictions.

On the other hand, the discovery of superconductivity at high temperature [3] held out a renewed inducement to the study of Josephson junction arrays. In fact, high-temperature ceramic superconductors, either in their polycrystalline form (that can be schematized by a disordered array of grains connected through point junctions [4]) or in their crystalline form (where, especially for the case of the most anisotropic materials, it has been possible to observe effects that are explainable as the coherent action of an ensemble of stacked junctions [5]), behave in several respects like arrangements of intrinsic junctions. In particular, properties such as continuous current conductivity, magnetic response or microwave absorption and generation can be understood in terms of the physics of weak couplings.

The study of the intrinsic Josephson effect is essential to the full understanding of the superconductivity mechanisms in high-T_c materials (see, for recent examples, [6]) and this effect is frequently invoked in the theoretical description of such systems [7]. Moreover, one of the features that make high-T_c superconductors especially hard to deal with is the strong effect of thermal fluctuations and defects, which results in a rather complex phase diagram. Josephson arrays appear again as suitable model systems for the modelling and comprehension of their behaviour.

In the recent past we have already devoted a review and a tutorial paper to the dynamical properties of a single vortex and to those of the ensembles of locked vortices [8]. Here, instead, we intend to give a (necessarily very simplified) overview of some recent works on the static properties of the arrays. Questions such as those of the nature of the ground states and their dependence on the physical parameters, and the description of the extremely rich phase space as a function of temperature (T), disorder (x), the applied magnetic field (f) etc will arise.

The review is organized as follows.

In sections 2 and 3 we review the theoretical background needed to describe the static properties of the JJAs. First, in section 2, we define the discrete JJA Hamiltonian and briefly comment on related models. Then we compare the discrete systems to the case of the superconducting thin films, pointing out results of general validity and differences. The mapping between the JJA Hamiltonian and Coulomb gas Hamiltonian is then presented.

In section 3 we complete the theoretical background, reviewing those elements of the scaling theory which are useful for extracting relevant information from experiments, and for comparing their results with theoretical predictions.

Section 4 is devoted to the discussion of the stable static solutions of the array; in particular, we will consider the ground-state problem. After a quick survey of the case of the superconducting thin film, we discuss in detail the problem of the ground-state configuration of the vortices when the JJAs are subjected to an external magnetic field. The section ends with a paragraph devoted to the problem of the stability of the different states.

In section 5 we make a point regarding the characterizing of the phase diagram of JJAs as a function of temperature (T), disorder (x), the applied magnetic field (f) and the anisotropy (η).

2. The discrete 'JJ array formalism'

2.1. The discrete JJA Hamiltonian

A Josephson junction array consists of a lattice of superconducting grains, connected to their nearest neighbours through Josephson junctions. The Hamiltonian of the system is given by

$$H = E_J\left(\sum_{ij}(1-\cos\phi_{ij}) + \frac{1}{2}\sum_{p,q}\Phi_{ind;p}\Lambda^{-1}_{p,q}\Phi_{ind;q}\right). \tag{1}$$

$E_J = \Phi_0 I_c/(2\pi)$ is the junction coupling energy, where I_c is the critical current and $\Phi_0 = h/2e$ is the elemental quantum of flux. $\phi_{ij} = \theta_i - \theta_j - a_{ij}$ is the gauge-invariant phase difference along the junction ij (restricted to the interval $(-\pi, \pi]$). θ_i is the phase of the pseudo-wave function describing the state of grain i: $|\Psi_i|\exp(\mathrm{i}\theta_i)$, where $|\Psi_i|^2 = n_s$ (n_s is the density of the superconducting couples). a_{ij} is related to the vector potential $\vec{A}$ through

$$a_{ij} = \frac{2\pi}{\Phi_0}\int_i^j \vec{A}\cdot\mathrm{d}\vec{x}.$$

ij stand for nearest-neighbour points and p, q run over all the plaquettes in the array.

The current along link ij is related to the phase difference ϕ_{ij} through the Josephson expression $\sin(\phi_{ij})$. An alternative description of the currents can be given in terms of mesh currents i_p, defined in each plaquette, which are related to the link currents by

$$\sin(\phi_{ij}) = (R^{\mathrm{T}})_{ij;p}i_p \tag{2}$$

where R is the discrete rotational operator. It is an $n_{cell} \times n_{link}$ matrix, where n_{cell} and n_{link} are, respectively, the number of cells and links in the array.

The self-induced magnetic field has been taken into account in order to provide a realistic description of the array [9]. This is just the interpretation of the second term in equation (1). The flux across a plaquette is due both to the self-induced and the external field (parametrized by the frustration, $f = \Phi_{ext}/\Phi_0$): $\Phi_p = \Phi_{ind;p} + 2\pi f$. $\Lambda_{p;q}$ is the adimensional full inductance matrix, normalized to $\Phi_0/(2\pi I_c)$. Its size is $n_{cell}\times n_{cell}$. Λ connects the induced magnetic flux through the plaquettes to the mesh currents defined on each cell:

$$\Phi_{ind;p} = \sum_{p,q}\Lambda_{p,q}i_q \tag{3}$$

and can be expressed as

$$\Lambda_{p,q} = \lambda_\perp^{-1}FF_{p,q} \tag{4}$$

where $\lambda_\perp$ is the adimensional effective penetration depth of the magnetic field [10]:

$$\lambda_\perp = \frac{1}{2\pi}\frac{\Phi_0}{\mu_0 I_c a} \tag{5}$$

where a is the lattice spacing of the array. $FF_{p;q}$ is a form factor matrix related to the geometry of the array. Details of its computation can be found in [8].

Fluxoid quantization can be expressed as

$$(R\phi)_p = -\Phi_p + 2\pi n_p \tag{6}$$

where Φ_p is the magnetic flux across cell p and n_p the number of vortices in that cell.

A further step towards a more realistic description of granular arrays is given by the introduction of disorder. This can be implemented by:

- Shift of the superconducting sites, which causes a deformation of the plaquettes in the array: they are not squares, and their area is not the same. Variation in the values of the cell areas, if the external magnetic field is uniform, results in the dispersion of the fluxes across the plaquettes: frustration is non-uniform, and matrix Λ is affected.
- Dispersion in the values of the critical currents.

As is well known, any vector field can be expressed as the sum of a solenoidal field plus an irrotational one (with vanishing divergence and curl, respectively). In our case, these two fields correspond to the site-like and plaquette-like variables (θ_i, Φ_p). Let us call the projector onto the solenoidal (irrotational) field P_r (P_d). It is trivially shown that $P_d = G(DG)^{-1}D$ (where G and D are the discrete versions of the operators gradient and divergence: G is an $n_{link} \times n_{site}$ matrix, where n_{site} is the number of sites in the array; it can be easily checked that $D = G^{\mathrm{T}}$). In a similar way we can define $P_r = R^{\mathrm{T}}(RR^{\mathrm{T}})^{-1}R$. Of course, $RG = 0$, $P_r P_d = 0$, $P_r P_r = P_r$, $P_d P_d = P_d$, $P_r + P_d = 1$. The London gauge ($\vec{\nabla} \cdot \vec{A} = 0$) implies that $(DG)^{-1}D\phi = \theta$, $(P_d\phi)_{ij} = \theta_i - \theta_j$ and $(P_r\phi)_{ij} = -a_{ij}$.

Applying the operator $(RR^{\mathrm{T}})^{-1}R$ to equation (2) and substituting into equation (3), it is possible to relate the induced field to the currents along the links. Thus, equation (1) can be entirely re-expressed in terms of gauge-invariant phases:

$$H = E_J\left(\sum_{ij}(1-\cos\phi_{ij}) + \frac{1}{2}\sum_{ij,kl}\sin\phi_{ij}L_{ij,kl}\sin\phi_{kl}\right) \tag{7}$$

where

$$L = R^{\mathrm{T}}(RR^{\mathrm{T}})^{-1}\Lambda(RR^{\mathrm{T}})^{-1}R. \tag{8}$$

Working with equation (1) implies solving a set of coupled non-linear equations. This is a hard business and one is usually forced to rely on numerical simulations to work out the problem. There are, however, analytical approximations which are rendered useful in particular cases; in the next subsection we will comment on the continuous limit of equation (1). Subsection 2.3 is devoted to the Coulomb gas model, which provides a complementary description of the arrays.

Throughout this paper we will focus on the sine-like dependence between the superconducting current (I_c) and phase (ϕ) typical of SIS (superconductor–insulator–superconductor) or SNS (superconductor–normal–superconductor) junctions. There has been recent interest, however, in SAS (superconductor–antiferromagnet–superconductor) junctions [11]. SAS junctions are calculated to be purely superconducting provided the phase shift is lower than a critical value ($\phi < \phi_c \Rightarrow I_c(\phi) \propto \phi$), while for $\phi > \phi_c$ the usual Josephson relation is reobtained, $I_c \propto \sin(\phi)$.

2.2. Superconducting thin films

There is a close analogy between Abrikosov vortices in superconducting thin films and vortices in Josephson arrays, defined by (6). As an example, the field profiles of an Abrikosov vortex

in a 2D superconductor (calculated from the London equation, with a penetration depth $\lambda_\perp$ much greater than the coherence length) and a Josephson vortex in a 2D array (obtained from simulation, with the same penetration depth) show an excellent agreement [12].

This idea suggests the use of the well-known analytical results obtained for the Abrikosov vortex Gibbs energy in 2D films as an approximation to that of a Josephson vortex in arrays. Its relevant terms are the energy of a vortex in the absence of magnetic fields and external currents, $U_0(x)$, and the energies due to the interactions with the external field and with the bias current, $U_f(x)$ and $U_i(x)$. Strictly speaking, U depends also on the vertical coordinate, y. Here, in order to simplify the discussion, we assume that the vortex moves along the central row of the array ($y = 0$).

The analytic expressions for $U_0(x)$ and $U_f(x)$ in terms of $E_J \equiv \hbar I_c/(2e)$ are given by [13]

$$U_0(x) = \pi \ln\left(\frac{2L}{\pi}\cos\left(\frac{\pi x}{L}\right)\right) \tag{9}$$

$$U_f(x) = -\frac{\pi^2 L^2}{2} f\left(1 - 4\left(\frac{x}{L}\right)^2\right). \tag{10}$$

x is given in units of the lattice spacing, a. We fixed the origin of the coordinates, $x = 0$, at the central column of the array. L is the array dimension in the direction perpendicular to the flow of the bias current.

A characteristic feature of Josephson arrays which is not present in 2D films is the periodic structure of the array. This implies that, in order to pass from one cell to the next, the vortex must overcome an energy barrier E_B. In order to take this into account we can consider an extra component of the energy

$$U_{pot}(x) = -\frac{1}{2} E_B \cos(2\pi x). \tag{11}$$

$U_{pot}(x)$ guarantees that there are equilibrium positions for a vortex in the array ($\mathrm{d}U/\mathrm{d}x = 0$) provided that it is not too close to the border.

Let us submit the previous expressions to scrutiny. Equation (9) reproduces qualitatively the behaviour of U in the absence of external fields. In figure 1(a) we have plotted the value of the energy of a vortex placed in the central plaquette $E(x = 0)$ for arrays with different sizes ($L = 16, 32, 64, 128, 200$). The points fit very well to a straight line $a + \pi \ln(2L)$ ($a \sim 0.059$).

The dependence on x is shown in figure 1(b), where we plot $\exp(g(\tilde{x}))$, with $g(\tilde{x}) = ((E(\tilde{x}) - E(0))/\pi)$, versus $\tilde{x}$; $\tilde{x} = x/L$ is a normalized length, ranging from 0 up to $1/2 - 1/L$. A perfect scaling is observed. The curve obtained differs from the expected cosine-like behaviour, while sharing two relevant qualitative features with it: it is convex and tends to 0 as $\tilde{x} \to 1/2$. Note that, though $E(\tilde{x}) = \pi \ln(2L/\pi g(\tilde{x}))$, there is no reason to fear a divergence of E in the limit $\tilde{x} \to 1/2$. The rightmost column of the array gives $x = (L - 1)/2$. The limit $\tilde{x} \to 1/2$ corresponds thus to $L \to \infty$. For $\tilde{x} \to 0.5$, g tends linearly to 0, $g(\tilde{x}) \to b(0.5 - \tilde{x})$ and $2L/\pi g(\tilde{x}) \to b/\pi$, which is non-zero.

The effect of frustration f is shown in figure 1(c). Unlike the behaviour predicted by equation (10), the energy of a vortex exhibits a parabolic dependence on f: it is minimum for a given value f_{min} and grows as f is increased or decreased. In figure 1(c) we plot the values of E for two vortices placed in diagonal plaquettes of a 32×32 array. For sufficiently high values of f the single-vortex configuration (while remaining stable) is no longer the ground state.

Things change when one takes into account the self-inductance of the array. It can be conveniently parametrized by the penetration depth $\lambda_\perp$. Negligible self-inductance corresponds to $\lambda_\perp = \infty$. As $\lambda_\perp$ decreases, so does the vortex extension and the effects of the

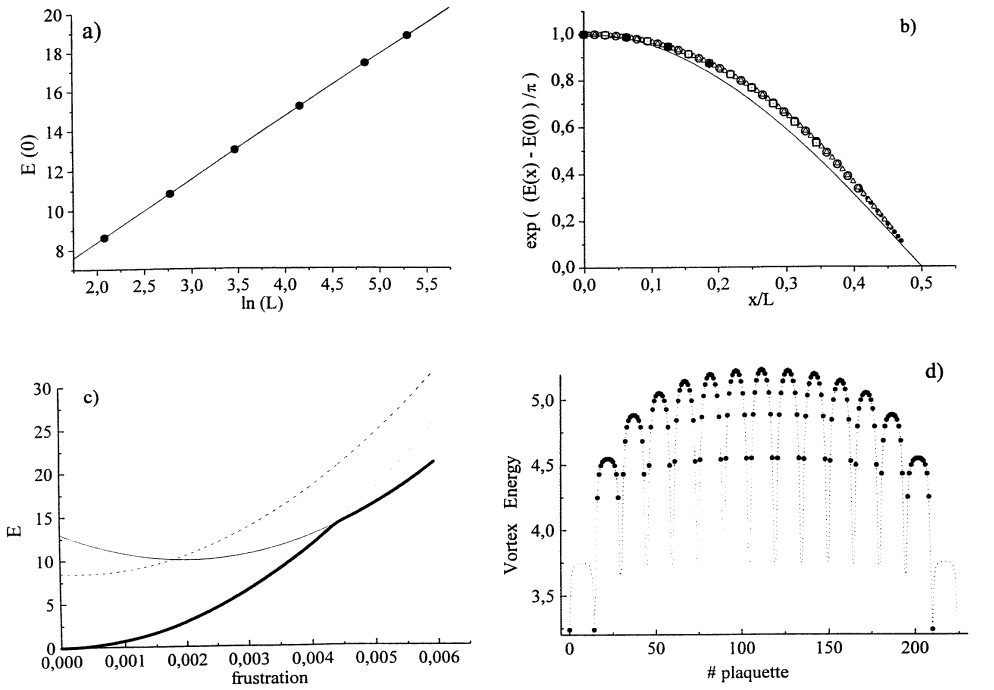

Figure 1. (a) $E(x = 0)$: the energy of a vortex placed in the central plaquette of a square $L \times L$ array versus $\ln(L)$; the straight line is $E = 0.059 + \pi \ln(2L)$. (b) $\exp(\{E(\tilde{x}) - E(0)\}/\pi)$ versus $\tilde{x} \equiv x/L$ for $L = 200$ (•), 128 (△), 64 (◯), 32 (□) and 16 (◇). A perfect scaling is observed. We also plot the expression predicted in the case of a superconducting film, $\cos(\pi\tilde{x})$ (continuous line). (c) The effect of frustration: the energy of one single-vortex configuration placed in different positions in a 32×32 array: the central plaquette (continuous line) and the leftmost (rightmost) one in the bottom row (dashed line); the dotted line is the energy of a zero-vortex configuration; the thick line is the envelope of the previous ones, and corresponds to the energy of the ground state. (d) The energy of a vortex as a function of its position for a 16×16 array with $\lambda_\perp = 1$. The cells are ordered from left to right, top to bottom (the leftmost cell on the top row is 0, the rightmost one on the bottom row is $(L-1) \times (L-1)$). We plot the values obtained from simulations (•) and from the expression $E_0 + E_{CG}$ (dotted line) (E_{CG} is equation (19) with $O \equiv (RR^{\mathrm{T}} + \Lambda)^{-1}$, and E_0 is just a constant term); despite all the approximations made in obtaining equation (19) and the finite-size effects, the relative error between the Coulomb gas results and the exact ones is always smaller than 1.5%.

array discretization become more and more apparent. Another consequence of the vortex shrinking is the flattening of the curve $E(x)$ [14]: the vortex extension decreases as $\lambda_\perp$ does; the presence of a very reduced vortex only affects the currents and field distribution in the plaquettes close to it, and the vortex profile attenuates considerably before arriving at the border of the array. Thus, across most of the array plaquettes (except those near to the border) the vortex energy is hardly sensitive to its position.

In conclusion, as $\lambda_\perp \to 0$ the 2D continuous model becomes less and less adequate, and another approach is required.

2.3. Mapping onto the Coulomb gas model

Hamiltonian (1) can be mapped onto the Coulomb gas model

$$H_{CG} = (q_R - f_R) P_{R,S} (q_S - f_S). \tag{12}$$

q_R is the occupation index of cell R: $q_R = 0$ means that there is no gas molecule in cell R; $q_R = \pm 1$ implies that the cell is occupied by a molecule with charge ± 1.

In this section we will provide an outline of the reason for this. For a rigorous proof, we refer the reader to reference [15]. We will approximate the cosine in the Hamiltonian (1) by the quadratic term (the general case will be discussed below)

$$1 - \cos(\phi_{ij}) \sim \frac{1}{2}\phi_{ij}^2 = \frac{1}{2}(\theta_i - \theta_j)^2 - (\theta_i - \theta_j)a_{ij} + \frac{1}{2}a_{ij}^2. \tag{13}$$

Due to the orthogonality of P_r and P_d, it is possible to decouple the site and plaquette fields. The summation over links can be expressed in terms of the previously defined operators as

$$\sum_{ij} \phi_{ij}^2 = \theta^{\mathrm{T}}\,\mathbf{\Delta}\theta + (R\phi)^{\mathrm{T}}(RR^{\mathrm{T}})^{-1}(R\phi) \tag{14}$$

where $\mathbf{\Delta} = DG$ is the discrete Laplacian. All of the information about the thermodynamic behaviour of the system is enclosed in the partition function

$$\begin{aligned} Z \equiv \int \prod_i [\mathrm{d}\theta_i]\ \exp\left(-\frac{\beta E_J}{2}\{\theta^{\mathrm{T}}\,\mathbf{\Delta}\theta\}\right) \\ \times \prod_p [\mathrm{d}\Phi_p]\ \exp\Bigg(-\frac{\beta E_J}{2}\{(\Phi - 2\pi n)^{\mathrm{T}} M(\Phi - 2\pi n) \\ + (\Phi - 2\pi f)^{\mathrm{T}} N(\Phi - 2\pi f)\}\Bigg) \end{aligned} \tag{15}$$

where $M = (RR^{\mathrm{T}})^{-1}$ and $N = \Lambda^{-1}$. RR^{T} is a Hermitian $n_{cell} \times n_{cell}$ matrix whose components are: $RR^{\mathrm{T}}_{p,p} = 4$, $RR^{\mathrm{T}}_{p,q} = -1$, if p and q are nearest-neighbour cells, and 0 otherwise. If periodic boundary conditions are imposed in all directions, matrix RR^{T} has a zero eigenvalue, so in order to calculate $(RR^{\mathrm{T}})^{-1}$ one must take the restriction of the operator to the subspace where the null eigenvector has been removed.

The integral over the site field gives a constant value:

$$\int \prod_i [\mathrm{d}\theta_i]\ \exp\left(-\frac{\beta E_J}{2}\{\theta^{\mathrm{T}}\,\mathbf{\Delta}\theta\}\right) = \left(\frac{2\pi}{\beta E_J}\right)^{o/2} \det(\mathbf{\Delta})^{-1/2} \tag{16}$$

where o is the order of the matrix $\mathbf{\Delta}$. In general, it is impossible to solve analytically an integral such as equation (16), and a series expansion around the maximum of the exponent is usually made.

In order to solve the integral over the plaquette field, it is convenient to do some calculations. If we introduce $y_p = \Phi_p - 2\pi f_p$, $a_p = 2\pi(n_p - f_p)$, then

$$\begin{aligned} &(\Phi_p - 2\pi n_p)M_{p,q}(\Phi_q - 2\pi n_q) + (\Phi_p - 2\pi f_p)N_{p,q}(\Phi_q - 2\pi f_q) \\ &\quad = (y - a)^{\mathrm{T}} M(y - a) + y^{\mathrm{T}} N y \\ &\quad = \xi^{\mathrm{T}}(M + N)\xi - a^{\mathrm{T}} M^{\mathrm{T}}(M + N)^{-1} M a + a^{\mathrm{T}} M a \end{aligned} \tag{17}$$

where $\xi = y - (M + N)^{-1}Ma$. If we define a new operator $O = -M^{\mathrm{T}}(M + N)^{-1}M + M$ (note that $(M^{-1} + N^{-1})O = 1$), the integral over the plaquette fields is just

$$\left(\frac{2\pi}{\beta E_J}\right)^{o/2} (\det(M + N))^{-1/2} \exp(-2\pi^2 \beta E_J (n - f)^{\mathrm{T}} O (n - f)). \tag{18}$$

We can define an effective Hamiltonian as

$$H_{eff} = 2\pi^2 E_J (q_p - f_p) O_{p,q} (q_q - f_q) \tag{19}$$

and equation (12) is obtained: the mapping to a Coulomb gas is achieved. Note that the charge-like variables q_p are exactly the fluxoids n_p.

In the (unrealistic) extreme case of $\lambda_\perp \to 0$, the induced field tends to counteract frustration ($\Phi_{ind} \to 2\pi(1-f)$ in the cell where the vortex is placed; $\Phi_{ind} \to -2\pi f$ otherwise), and $\phi_{ij} \ll 1$ [16]. Thus the approximation $\cos(\phi_{ij}) \sim 1/2\phi_{ij}^2$ is reasonable.

For realistic values of $\lambda_\perp$, the Hamiltonian (19) (with $q_p = n_p$) also provides an acceptable description of the system, as shown in figure 1(d) for $\lambda_\perp = 1$.

Now we state the main results obtained through a rigorous development: in the case of the wire model (similar to that previously solved: $H \propto \sum \phi_{ij}^2$) the phase-like and vortex-like variables are decoupled, and the partition function can be expressed as the product

$$Z = Z_{SW} Z_{ch}. \tag{20}$$

Z_{SW} is the partition function of the spin waves, and takes into account the quadratic fluctuations around an equilibrium state. Z_{ch} is analogous to the previously obtained Coulomb gas effective Hamiltonian (equation (19)). We stress that the identity between charge variables q_p and the fluxoids n_p persists.

If periodic boundary conditions are imposed in all of the directions, the following constraints arise:

$$\sum_p q_p = 0 \qquad \sum_p f_p = 0 \tag{21}$$

where the summations are over all the plaquettes in the array. When working in three or more dimensions, another constraint must be considered: as q_p and f_p are defined as curls of a vector field, their divergence must be zero:

$$\vec{\nabla} q = 0 \qquad \vec{\nabla} f = 0. \tag{22}$$

In the general case, the potential in equation (13) is usually substituted for with the Villain potential [17], defined as

$$V_v(x) = -\frac{1}{\beta} \ln \sum_{l=-\infty}^{\infty} \exp\left(-\beta \frac{J_v}{2} (x + 2\pi l)^2 \right). \tag{23}$$

Note that both the piecewise-parabolic potential and the cosine ($V(x) = \cos(x)$) are the limits of the Villain potential in the cases of high and low temperature, respectively (see figure 2). The partition function obtained from the Villain potential leads to results formally equivalent to equations (19) and (20). The difference is that now the Coulomb gas Hamiltonian is expressed in terms of charges (q_p) whose relation with the vorticity of the plaquettes (n_p) or any function of the initially defined phases is non-trivial. In particular [18],

$$\langle (RV')_p (RV')_q \rangle = \langle q_p q_q \rangle. \tag{24}$$

The second average is made considering the Coulomb gas Hamiltonian, and q_p, q_q are the charge variables in the cells p, q. The first average is calculated integrating over the ϕ-variables, using Villain's potential, and R is as usual the discrete rotational:

$$(RV')_p = \sum_{ij \in p} V'(\phi_{ij})$$

where

$$V'(\phi) = \left(2\pi \sum_{l=-\infty}^{\infty} \exp\left(-\frac{\beta J_v}{2} (\phi + 2\pi l)^2 \right) \right)^{-1} \sum_{l=-\infty}^{\infty} \mathrm{e}^{-(1/2)\beta J_v (\phi + 2\pi l)^2} (\phi + 2\pi l). \tag{25}$$

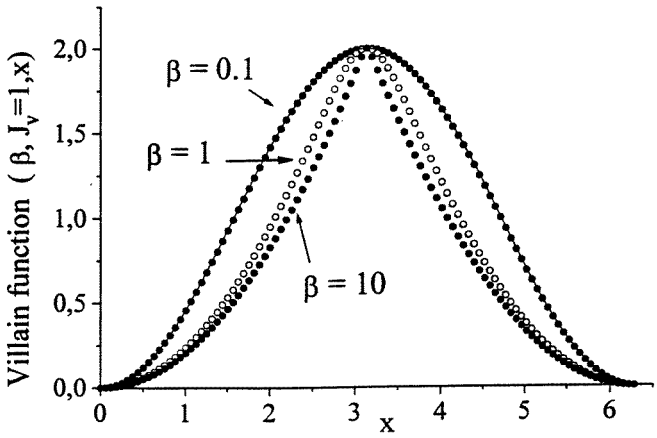

Figure 2. The Villain potential (V_v) for different values of β: 0.1, 1 and 10 ($J_v = 1$). In particular, we have plotted the function $a(V_v(x) - b)$, taking $b = V_v(0)$ and $a = 2/(V_v(\pi) - V_v(0))$. a and b are β-dependent. For comparison we have added the curve $1 - \cos(x)$ (continuous line). Note that the piecewise-parabolic function and the cosine are limits of V_v for high and low values of β, respectively.

2.4. Related models

In section 2.1 we have considered the so-called *frustrated XY model*, to which self-inductance and disorder effects have been added. Thus a rather complex model, containing many of the features found in real systems, is obtained. Sometimes it is useful to rely on more basic models that reflect partially that complexity and allow an easier overview on particular aspects of the problem to be obtained, and/or allow one to benefit from a whole body of intuitions and ideas about order, stability etc that theoreticians have developed through the years.

- *Gauge glass*: either in its phase (equation (1)) or vortex (equation (19)) representation, it is characterized by the uniform distribution of the vector potentials a_{ij} in the $[0, 2\pi]$ interval. In equation (1), this implies that the p-component of the $R\phi$-vector takes any value between 0 and 8π with the same probability. In equation (19), f_p can have any value within the [0, 4] interval.

  This model corresponds to a fully non-uniform flux distribution. It exhibits U(1) symmetry (is invariant under a global shift of all the phases).

  At low enough temperatures, this model undergoes a transition to a phase-correlated ordered state.
- *Chiral glass*: in this model, the vector potential a_{ij} can only take two possible values, both equally probable: 0 and π. The non-linear component of the Hamiltonian (equation (1)) becomes $-E_J \cos(\phi_{ij}) = -E_J \cos(\theta_i - \theta_j - a_{ij}) = \pm E_J \cos(\theta_i - \theta_j)$. This model can be seen as a representation of the XY spin glass with couplings $K_{ij} = \pm E_J$. It is worth noting that a negative Josephson coupling can arise from pair hopping through a Kondo singlet, as shown in the strong-coupling limit of the 1D Kondo lattice [19].

  In the vortex representation (equation (19)), f_p has only a discrete set of possible values.

  This model shares a relevant qualitative feature with the XY model with rational values of f. They are both invariant under two kinds of transformations, exhibiting a continuous U(1) symmetry, and a discrete one (Z_q for the XY model with $f = p/q$, and a global reflection $\theta_i \to -\theta_i \ \forall i$ in the case of the chiral glass).

At a low enough temperature, this model undergoes a transition whose order parameter is the chirality $\chi = \sum_{ij}(\theta_i - \theta_j - a_{ij})$ (the sum is taken around the links of each plaquette). In 3D, gauge glass and chiral glass belong to the same universality class [20]: despite the differences between the two models, their transitions are characterized by the same critical exponents. However, in 2D they exhibit different critical behaviours [21].

- *Bond dilution* is an extreme case of distribution of the critical currents: they have two possible values: 0 and a unique I_c. In 2D, it is suggested to be in the same university class as gauge glass [22].
- Other proposals are inspired by the physical realizations of disordered superconductors. For example, a random-pinning Hamiltonian has been suggested in reference [23]:

$$H_{rp} = -\frac{1}{2}\sum_{p,q}(n_p - f)G(p-q)(n_q - f) - \sum_p v(p)n_p^2 \tag{26}$$

where p and q run over all the plaquettes in the array. In this Hamiltonian, the flux is constant over the whole array (reflecting the physical situation of having a uniform applied magnetic field) and the distribution of the values of $v(p)$ reproduces the pinning effect due to array defects.

In 2D, this potential belongs to the same universality class as gauge glass [23].

A summary of the universality behaviour of the different models considered in this paper is given in figure 3. These results will be commented on in detail in section 5.

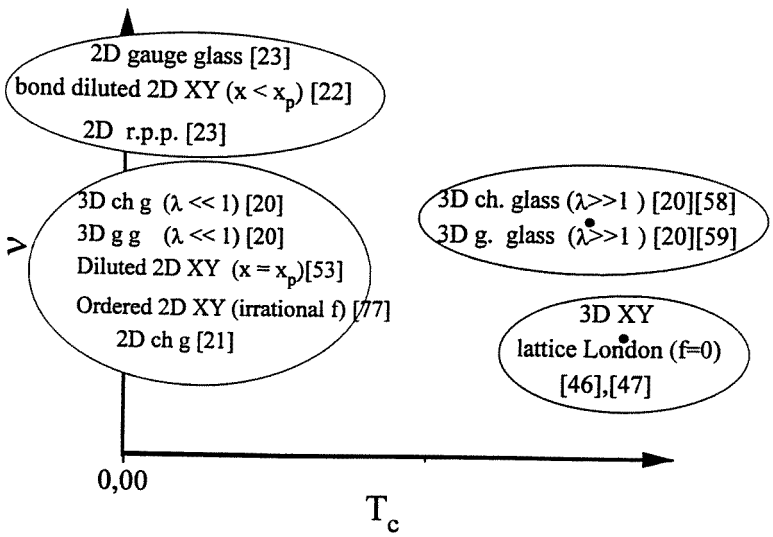

Figure 3. Different models commented on in this paper, classified according to their transition temperature (zero or finite) and their static exponent ν. 'ch g', 'g g' and 'r.p.p.' stand, respectively, for chiral glass, gauge glass and the random-pinning potential defined in reference [23].

3. Review of scaling theory

In this paper we are dealing with the static properties of the JJ (such as phase diagrams concerning transitions between different phases). However, experiments are usually made under dynamical conditions (e.g. injecting a bias current and studying the I–V curve). These

experiments report useful information on the physics of the array: the proximity to a phase transition gives rise to remarkable features in the I–V characteristics, the appearance of non-linear resistivity can be related, e.g., to the exponent with which the correlation length diverges near a transition. This is why it is convenient to briefly review some notes on scaling theory regarding I–V behaviour in the vicinity of a second-order phase transition. For further development, we refer the reader to references [24, 25].

A second-order phase transition is characterized by the development of long-range correlations, which can be described in terms of a power divergence of the correlation length in the vicinity of the transition:

$$\xi \sim (T - T_c)^{-\nu}. \tag{27}$$

The relaxation time also diverges as one approaches the critical point. The characteristic timescale (τ) is defined as

$$\tau \sim \xi^z. \tag{28}$$

If $T_c = 0$, however, the relaxation is expected to diverge exponentially as $T \to 0$, which implies $z \to \infty$: $\tau \sim \exp(\Delta E(T)/T)$, where $\Delta E(T)$ is the typical energy barrier that a vortex must overcome to move a distance ξ. The dependence of $\Delta E(T)$ on ξ is usually expressed through the introduction of a new exponent ψ such that $\Delta E \sim \xi^{\psi}$ and

$$\tau \sim \exp(A/T^{1+\psi\nu}). \tag{29}$$

The vector potential A enters in the a_{ij}-definition as an inverse length, so it is expected to scale as the inverse of the relevant length scale, ξ:

$$A \sim \frac{1}{\xi}. \tag{30}$$

The electric field is defined as $E = -\partial A/\partial t$. Thus, it presumably must scale as $1/(\text{length} \times \text{time})$, so

$$E \sim \frac{1}{\xi\tau}. \tag{31}$$

The power dissipated per unit volume is $IV/L^d = JE$ (d is the dimension of the system, J is the current density and E the electric field). JE scales as energy/(time $\times$ length^d); thus $EJ \sim K_B T/(\xi^d \tau)$. From equation (31), this implies

$$J \sim \frac{K_B T}{\xi^{d-1}}. \tag{32}$$

From equations (31) and (32) we obtain the scaling *ansatz*

$$E\xi\tau \sim f_{\pm}\left(\frac{J\xi^{d-1}}{K_B T}\right) \tag{33}$$

where $\pm$ indicates possibly different behaviour above and below the critical point.

Dividing both terms by $J\xi^{d-1}/(K_B T)$ one obtains

$$T\tau\xi^{2-d}\frac{E}{J} \sim g_{\pm}\left(\frac{J\xi^{d-1}}{K_B T}\right). \tag{34}$$

At very low currents, E is linear in J; thus an ohmic behaviour occurs. The linear resistivity ρ_{lin} is defined as $\rho_{lin} = \lim_{J\to 0} E/J$; thus $\rho_{lin} \sim (T\tau)^{-1}\xi^{d-2} g_{\pm}(0)$, and

$$T\rho_{lin} \sim \xi^{d-2}\exp(-A/T^{1+\psi\nu}) \qquad T_c = 0 \tag{35}$$

$$T\rho_{lin} \sim \xi^{d-2-z} \sim |t|^{\nu(z+2-d)} \qquad T_c \neq 0 \tag{36}$$

where $t = T - T_c$. Consequently

$$\frac{E}{J\rho_{lin}} \sim g\left(\frac{J}{T^{1+\nu(d-1)}}\right) \qquad T_c = 0 \tag{37}$$

$$\frac{E}{J\rho_{lin}} \sim g_{\pm}\left(\frac{J}{T|t|^{\nu(d-1)}}\right) \qquad T_c \neq 0. \tag{38}$$

Equations (37) and (38) show that the I–V (J–E) curve is different at different temperatures, but all the different curves coincide just on re-scaling $I \rightarrow I/(T^{1+\nu(d-1)})$ or $I \rightarrow I/(|t|^{\nu(d-1)})$. This gives us a clue as to how to search for vestiges of a second transition and to determine critical exponents from I–V curves.

For example, above a given current $I_{nl}(T)$, the I–V curve is no longer a horizontal line, and non-ohmic behaviour comes into play. The point of the curve where non-linear behaviour sets in scales (for $d = 2$, in the $T_c = 0$ case) as

$$I_{nl} \sim T^{1+\nu}. \tag{39}$$

A new difficulty arises when working with small systems (one is forced to do this when simulating systems for dimension $d > 2$). In this case, finite-size scaling is mandatory. This just takes into account the fact that the maximum coherence length is reached when $\xi \sim (T - T_c)^{-\nu}$ is of the order of the system size L: $\xi \sim L$. The main idea underlying finite-size scaling is that, as regards length scales, only the ratio L/ξ is relevant. In order to compare results obtained for those systems, formulae must be corrected to take this into account. For example, equation (37) must be generalized to

$$\frac{E}{J\rho_{lin}} \sim g\left(\frac{J}{T^{1+\nu(d-1)}}, L^{1/\nu}T\right). \tag{40}$$

and equation (39) to

$$\frac{I_{nl}}{T^{1+\nu}} \sim g\left(\frac{J}{T^{1+\nu}}, L^{1/\nu}T\right). \tag{41}$$

If $T_c \neq 0$, $T\tau\rho_{lin} \sim \xi^{d-2}$ can be read as $\rho_{lin} \sim \xi^{d-2-z}$ (T can be taken to be a constant near T_c, while the other parameters are functions of $T - T_c$). The finite-size scaling reads now

$$\rho_{lin} \sim \xi^{d-2-z} g_{\pm}(L^{1/\nu}|t|). \tag{42}$$

Comparison between systems with different lengths, L and L', leads to

$$\frac{\ln(\rho_{lin}(L)/\rho_{lin}(L'))}{\ln(L/L')} = d - 2 - z \tag{43}$$

at $T = T_c$.

4. The ground-state problem

When studying the ground-state configuration of a superconducting array, an immediate reference (a *not-too-different* system whose analytical solution is known) is a continuous superconducting film. We will first briefly review some basic properties of such a model, which can be considered as the limit of a discrete array for very low frustration ($f \rightarrow 0$). Next we will consider how discretization makes things change.

4.1. Superconducting film

The mean-field solution minimizing the Ginzburg–Landau free energy of a thin film is very similar to that found in 3D [26]. The ground-state configuration is a triangular lattice of equally spaced vortices, whose areal density is B/Φ_0, and their average separation is $\sqrt{(\Phi_0/B)}$. Fluctuations about the ground state can be worked out by using the London approximation: outside the vortex core, the amplitude of the superconducting wave function is fixed, and only the phase fluctuates (this is a reasonable approximation if the vortex size is much smaller than the average separation between vortices). What one obtains with this approximation is

$$H = \frac{1}{2} J_0 \int \mathrm{d}^2 r \left| \nabla\theta - \frac{2\pi}{\Phi_0} A \right|^2 . \tag{44}$$

Equation (44) can be mapped onto a continuum Coulomb gas of logarithmically interacting charges [27]. For finite B, the resulting Hamiltonian can be written as [28]

$$H = \frac{1}{2} \int \mathrm{d}^2 r \; \mathrm{d}^2 r' \; (n(r) - B/\Phi_0) V(r - r')(n(r') - B/\Phi_0) \tag{45}$$

where $n(r) = \sum_i n_i \delta(r - r_i)$ ($n_i = \pm 1$ is the vorticity of vortex number i, and r_i its position). Equation (45) is just the continuum limit of equation (12). A continuum film is the limit of a discrete 2D array when its spacing $a \to 0$. Since the average number of vortices per plaquette is $f = a^2 B/\Phi_0$, the $a \to 0$ limit implies $f \to 0$.

4.2. The discrete 2D array

How does discretization make things change? In a discrete 2D array two tendencies compete: vortices tend to organize in triangular patterns but, at the same time, they are trapped in a periodic potential whose minima are placed at the plaquettes of the array. When the geometry of the array is incommensurate with a triangular structure (e.g. for square plaquettes) this competition gives rise to an extremely rich ground-state structure as a function of the array size and the frustration. In square arrays, for low values of f, vortices search for the approximation to a triangular lattice that fits better within the array geometry, and thus the ground-state configurations depend strongly on the exact value of f: they change notably as f changes.

One way of obtaining the ground-state configuration is starting from a triangular vortex lattice and subjecting it to rotation and shear, so as to adapt it to the square geometry of the array. In this way, for $f = 1/q$ a Bravais lattice of vortices emerges, characterized by a periodic structure whose basic cell contains $q \times q$ plaquettes [29] (see figure 4). In some special cases, however, the basic cell is $2q \times 2q$ (currents are spatially periodic, with period q, but gauge-invariant phases exhibit a $2q$-periodicity) [30].

The complexity of determining the ground state is perfectly illustrated in the exhaustive and rigorous work by Straley and Barnett [30], where different candidate ground states are exhaustively searched for by first selecting candidates among local minimum configurations, moving the vortices around in search of lower-energy arrangements, finding via Monte Carlo simulations competing structures and *a posteriori* demanding the internal consistency of the resulting classification scheme and checking systematic regularities of the configuration properties with f. In this way, a complete classification scheme emerges:

(a) in general, Bravais lattices are a good description for the $f = 1/q$ ground states;
(b) for other values of f, the ground state is given by domains corresponding to a Bravais configuration between which domain walls or narrow bands corresponding to a different configuration are inserted. For $1/3 < f < 1/2$ the structures obtained are made just by inserting $f = 1/3$ configuration domains in the $f = 1/2$ checkerboard configuration.

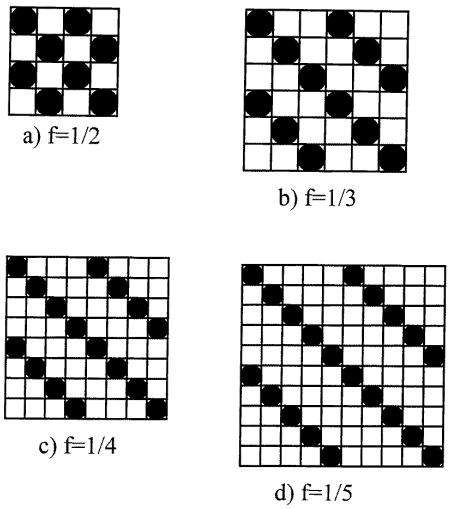

Figure 4. Bravais ground-state configurations for $f = (a)$ 1/2, (b) 1/3, (c) 1/4 and (d) 1/5. Vortices are represented by black circles.

This results, in most cases, in a diagonal chain of vortices with a staircase-like invariance, as evidenced by Halsey [29].

In particular, near $f = 1/q$ the ground state is the configuration for $1/q$ onto which a dilute configuration carrying the excess vortices/vacancies is superimposed [31]. In [31], ground states have been worked out by studying one by one all of the possible vortex configurations (after discarding the ones that are redundant because of translational and inversion symmetry), searching that with the minimum energy (a Coulomb gas Hamiltonian is considered) and checking them by means of slow Monte Carlo cooling from random configurations at high temperatures. The unbinding of these superimposed vortex arrays occurs at critical temperatures lower than those characteristic of $f = 1/q$; thus the critical temperature pattern exhibits a rich structure.

A useful method for identifying the ground states has been proposed by Kolahchi [32], inspired by the growth of large crystals: local minimum configurations are singled out in a ladder; then they are replicated in a new ladder, which is added to the initial one, and phases are allowed to relax. It is found that, in passing from one ladder to the next one, a general rule of shifting phases applies. Finally the configuration for the square array is obtained. Ground states are expected to be between the minima so calculated.

Anyway, the process of finding out the candidates for ground states and discriminating between them is rather cumbersome. Finding the exact ground-state configuration for a given set of the parameter values is fairly arduous work. This is partly due to the glassy nature of the system, characterized by a complex structure of metastable states, nearly degenerate in energy with the real ground state, and by constrained dynamics (the different energy minima are dynamically disjoint: each of them is unreachable from the others, because that would require the rearrangement of an infinite part of the vortex lattice). Another serious difficulty arises from the requirement of considering $q \times q$ arrays so that the ground-state configuration is commensurate: this imposes a serious computational limit for the simulation of small values of f. New difficulties arise when trying to take into consideration the magnetic fields induced by the supercurrents circulating in the array.

A more general method—other than trial and error—would be highly desirable. One such method has been worked out in the case of ladders in reference [33]. The symmetry between the currents flowing along the upper and lower branches of the ladder allows one to map the system onto a 1D chiral XY model with anisotropy. This model belongs to a general class of 1D models with spatially modulated structures, such as the Frenkel–Kontorova (FK) one, which has been exhaustively studied [34]. However, applying the well-known results obtained for the FK model to the ladder is far from trivial. The equilibrium properties of these 1D models depend strongly on the convexity of the interaction potential: in the FK model, V is clearly convex ($V(x_i, x_{i+1}) = k(x_i - x_{i+1})^2$), while the cosine-like potential of a ladder has a non-convex part. However, it can be proved [35] that only the convex part of V is relevant in determining the ground-state configurations, and the ladder ground states exhibit the same properties as the convex models; thus all the results and techniques previously developed for these models can be applied to ladders. In reference [35] one such technique, the *effective-potential method*, was applied. It is based upon the study of the transfer matrix of the system partition function, and allows one to compute the ground states with an arbitrary accuracy. When applied to the ladder, this method finds a rich ground-state structure as a function of frustration f. The vortex density $w(f)$ climbs a Devil's staircase: it is a continuous function, with a plateau for rational values of f. This clearly differs from the behaviour of a 2D array, where $w(f) = f$ everywhere [29]. In particular, the occupation index of a plaquette in the ladder is given by $n_i = \kappa_w(\mathrm{i}w + \alpha)$, α being an arbitrary constant, and the function $\kappa_w(x)$ is defined on the [0, 1] interval as $\kappa_w(x) = 1$ for $x < w$ and 0 otherwise. Moreover, anisotropic ladders are considered. The anisotropy is parametrized by J_t, which is the ratio between the vertical and horizontal coupling constants: $J_t = E_{JY}/E_{JX}$. The ground-state phase diagram in the J_t–f plane is composed of a series of tongues, each corresponding to a different vortex density w (see figure 5).

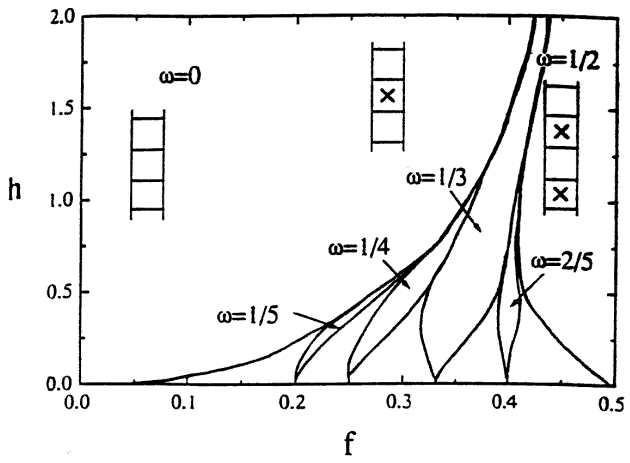

Figure 5. The ground-state phase diagram for a ladder as a function of frustration (f) and anisotropy ($h = J_y/J_x$), obtained by the effective-potential method. w is the number of vortices per cell. Vortex configurations for simple values of w are shown in the inset. Courtesy of Mazo, Falo and Floria [33].

Independently, a different group [36] arrived at similar conclusions. They showed that the Devil's staircase varies with the anisotropy parameter J_t: for $J_t < 0.7$, $w(f)$ shows flat regions, corresponding to rational values of f, connected by smooth differentiable curves. At

$J_t = 0.7$ the staircase is complete (there is a step for every rational f, and the measure of the curve pieces corresponding to irrational f is zero). For $J_t > 0.7$ the staircase is overcomplete (steps for $f = p/q$ with lower q increase, and those for higher q shrink; in the limit $J_t \to \infty$ only integer steps survive).

The effect of the self-induced magnetic field has been studied in reference [16]. The effective-potential method was used, combined with other techniques, such as root-finding methods (calculating stable solutions to $\partial H/\partial x_i = 0$) and dynamical relaxation. In the self-field, the system presents a behaviour that resembles the Meissner effect: the self-induced field tends to push the external field out of the array, causing the growth of the $\omega = 0$ tongue and the shrinking of the range of parameters where the Devil's staircase is observed. However, the critical field for the $\omega = 0$ phase (the frustration above which the configuration is no longer the ground state) remains lower than $\frac{1}{2}$ for all of the values of the penetration depth (this has been analytically checked for the extreme case $\lambda_\perp \to 0$). Thus commensurate phases with vortices are always clearly visible in the phase diagram and the Devil's staircase structure is maintained for any value of $\lambda_\perp$.

4.3. Stability

An appealing question is that of the robustness and stability of the equilibrium configurations under variation of the external parameters. It provides relevant information on the energy landscape of the system and its dynamical behaviour (constrained dynamics, slow relaxation processes etc). Stability analysis can be related to depinning, which occurs when a given static vortex configuration loses its stability as a result of variation of the external current, the applied magnetic field etc [37]. On the other hand, the loss of stability of the zero-vortex ($w = 0$) configuration as frustration is raised starting at $f = 0$ has been studied as a guess at the mechanism of field penetration [38]. Furthermore, remarkably the study of the stability of the static states has been recently proved to be relevant to the understanding of such an attractive dynamical phenomenon as row switching [39]. Row-switched (RS) states are characterized by the motion of vortices along well-localized channels in the array: the rest of the rows remain in the superconducting state. Thus two different regions can be clearly distinguished in the array: 'switched rows' (S) exhibiting a non-zero voltage, and 'quiescent rows' (Q), with zero voltage. For given values of f and β_c there exists a current range $i_{ext} \in (i_{min}, i_{max})$ where row switching occurs. The upper current limit i_{max} is shown to be given by the loss of stability of the superconducting state in a Q-region: starting from a given RS state, as the injected current increases there is a moment when vortices penetrate a Q-region; this results in a new RS state and eventually, for $i = i_{max}$, in the disappearance of the RS phenomenon. (The authors of [39] argue that the lower current limit i_{min} is due to a completely different mechanism, namely retrapping, which explains the dependence of RS on the damping parameter β_c.)

A static configuration is characterized by $\partial H/\partial\phi_{ij} = 0$ for every ϕ_{ij}. Furthermore, if the second-derivative matrix K, given by $K_{ij;kl} = \partial^2 H/\partial\phi_{ij}\,\partial\phi_{kl}$, is positive definite, the configuration is stable. In the case of Hamiltonian (1), matrix K is just

$$K = \mathbf{Cos} + R^{\mathrm{T}}\Lambda^{-1}R \tag{46}$$

where **Cos** is a diagonal $n_{link} \times n_{link}$ matrix whose (ij, ij) component is just $E_J \cos(\phi^*_{ij})$ (ϕ^*_{ij} is the gauge-invariant phase shift corresponding to an equilibrium configuration). This result permits us to understand the effect of self-inductance on the stability of a given vortex configuration. In the limit $\lambda_\perp \to \infty$, screening is negligible and thus $K = \mathbf{Cos}$. Let us start from a stable configuration at a given value of f, where all the phases are such that $0 < \phi_{ij} < \pi/2$. Thus, all the components of K are positive, and K is positive definite. As f

varies there may be a moment when one of the phases reaches its maximum value $\phi_{ij} = \pi/2$; at this point, K is no longer positive definite ($\det K = 0$) and the configuration becomes unstable. This behaviour has been pointed out by several authors for a ladder [33, 40]: once the supercurrent in one link reaches its maximum value, no change in the field can be sustained by an increase of the currents and the vortex structure becomes unstable, so the system relaxes to a new vortex configuration.

The effect of self-inductance on stability comes through the matrix $R^{\mathrm{T}}\Lambda^{-1}R$. It is a real, symmetric, positive-definite matrix. In the limit of a very strong screening ($\lambda_\perp \to 0$) the self-induced field is able to counteract the external one, and the resulting equilibrium phases are $\phi_{ij} \sim 0$ [16]; thus **Cos** is also positive definite and any vortex configuration is stable. For finite values of $\lambda_\perp$, the expected effect is the increase of the range of f-values where any vortex configuration is stable. This was explicitly checked for ladders [16] and 2D arrays [38] (for the case of a ladder, see figure 6).

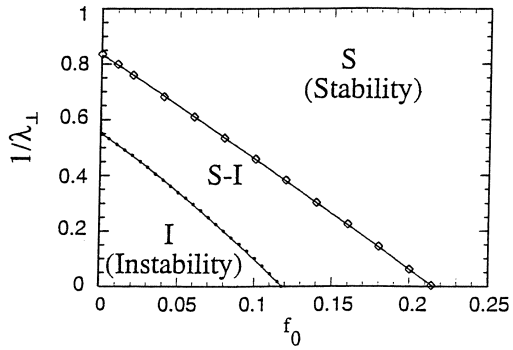

Figure 6. The border between stability and instability regions in the parameter space for the extreme cases of one single vortex (black points) and the $w = 1/2$ configuration (rhombi) in an isotropic ladder. In the first case we have considered a 128-cell ladder. We define $\lambda_{\perp c}(0)$ as the penetration depth below which a configuration is stable at $f_0 = 0$, and f_c as the value of the frustration below which a configuration is no longer stable in the limit of no inductance ($\lambda_\perp \to \infty$). For a configuration with one single vortex, $f_c = 0.1175 \pm 0.000\,65$ and $\lambda_{\perp_c}(0) = 1.812 \pm 0.018$; in the $w = 1/2$ case, $f_c = 0.215 \pm 0.001$ and $\lambda_{\perp_c}(0) = 1.197 \pm 0.006$. Note that, unlike the behaviour of a 2D array, in a ladder with no self-inductance effects, there exists a critical value of the field for the stability of each phase: for $f_0 < f_c(\omega)$ the phase ω is no longer stable. Courtesy of Mazo and Ciria [16].

The stability of a given configuration has recently been studied by considering a dynamical algorithm in reference [37], where similar results (in the $\lambda_\perp \to \infty$ case) were obtained. The argument used in this reference can be applied to a system with non-negligible self-inductance: starting from an equilibrium configuration $[\phi^*]$, a small perturbation is added to the phases: $\phi^*_{ij} \to \phi^*_{ij} + \alpha_{ij}$. The dynamical equations of the array are, in a matrix expression [8],

$$\beta_c\ddot{\phi} + R_c\dot{\phi} + \mathbf{i}_c\,\mathbf{Sin} + R^{\mathrm{T}}\Lambda^{-1}R\phi + A\mathbf{i}_{ext} + 2\pi R^{\mathrm{T}}\Lambda^{-1}R\mathbf{f} = 0. \tag{47}$$

Here β_c, R_c and $\mathbf{i}_c$ are diagonal $n_{link} \times n_{link}$ matrices, introduced so as to allow some dispersion in the values of capacitances, resistances and critical currents. A is an $n_{link} \times n_{site}$ non-symmetric matrix, and **Sin** is a diagonal matrix whose (ij, ij) component is just $E_J \sin(\phi^*_{ij})$. From equation (47) the perturbation evolves as

$$\beta_c\ddot{\alpha} + R_c\dot{\alpha} + K\alpha = 0 \tag{48}$$

where K is defined in equation (46). Reference [37] concludes that the stability of the solutions occurs if and only if the stiffness matrix K is positive definite, independently of matrices β_c,

R_c and $\mathbf{i}_c$. As expected, the 'statical' and 'dynamical' criteria for stability are exactly the same. Provided that a phase configuration is nearly enough an equilibrium one, any algorithm (minimizing H or letting the system evolve following the dynamical equations) will result in the same final state.

5. Phase diagram

As commented on in the introduction, one of the features that make high-T_c superconductors especially hard to deal with is the strong effect of thermal fluctuations and defects. For example, the perfect (no defect) type-II superconductor phase diagram (see figure 7) with the Meissner–

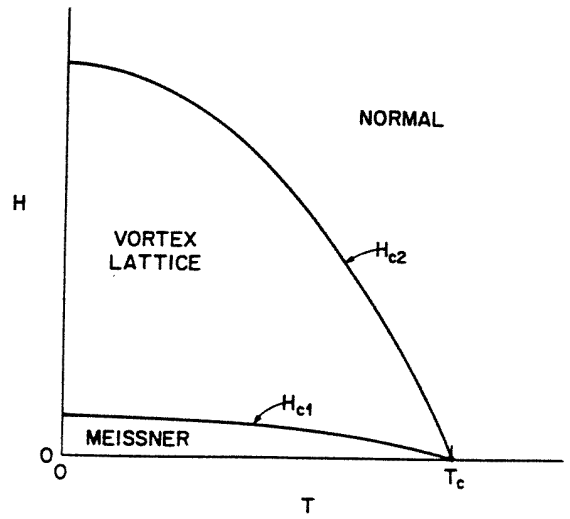

(a)

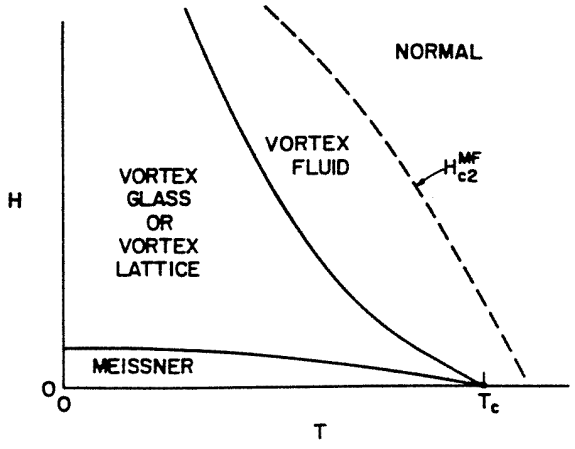

(b)

Figure 7. (a) The mean-field phase diagram of a type-II superconductor. (b) The phase diagram of a 3D type-II superconductor with strong thermal fluctuations. Courtesy of Fisher, Fisher and Huse [24].

Abrikosov vortex lattice and normal phase is no longer valid [24]. Strong thermal fluctuations make this diagram change drastically. Part of the f–T plane is occupied by a vortex fluid phase. In this phase there is a tendency to local pinning of vortices, but the pinning field strongly fluctuates with a finite correlation length. The system can be described in terms of moving, fluctuating vortices. This is a fully disordered phase, and thus is not separated from the normal phase (no local pairing) by a proper transition, but rather by a smooth crossover, which is placed near the mean-field f_{c2}-line. In normal and vortex fluid phases the Lorentz force due to any applied current makes the flux lines move, producing a non-zero V. At lower T, however, a transition to a state with vanishing resistance occurs: defects can pin vortices, impeding their movement. This zero-resistance state is referred to as vortex glass. It is characterized by:

- as mentioned, vortices being pinned to the lattice defects, and $R = 0$;
- the positions of the defects being random, and thus there being no long-range order in the vortex lattice (for dimensions $d < 4$).

The vortex liquid–vortex glass transition line lies very close to the upper critical field in conventional low-T_c materials. The liquid phase occupies a large part of the f–T phase diagram for highly anisotropic materials, such as Bi–Sr–Ca–Cu–O. The transition line is of the form $f_g \sim (1 - T/T_c)^n$, where n strongly depends on the material under consideration: for cuprates $n \sim 3/2$ at high temperatures and rapidly varies with decreasing temperature [41], while for cubic (K, Ba)BiO_3 superconductors n remains constant at $3/2$ over three decades of T-values [42].

At even lower T, the bulk superconductor is able to expel the applied magnetic field completely: the system is in the Meissner phase.

Simulations and experiments on Josephson junction arrays are of great utility for the comprehension of such a complex phase diagram. An example of the successful use of a JJA system to reproduce the behaviour of bulk high-T_c superconductors is related to the order of the critical transitions. In fact, while in clean (perfectly ordered) superconductors the vortex lattice–vortex fluid transition is (supposedly) of first order, for strong enough disorder the vortex glass–vortex fluid transition becomes continuous. This behaviour is reproduced in Josephson arrays: in 3D ordered arrays the superconducting transition occurs through a first-order melting of the vortex lattice [43], while a high enough level of disorder is seen to destroy this first-order transition, transforming it into a continuous one [44]. In particular, the Meissner transition in zero applied field in a high-T_c superconductor is widely accepted now to be in the same universality class as the 3D XY model [45]. This picture is supported by simulations of the lattice London superconductor model, whose Hamiltonian is defined as

$$H = \sum_{i,\vec{\mu}} \left\{ U(\theta_{i+\vec{\mu}} - \theta_i - \lambda_0^{-1} a_{i,\vec{\mu}}) + \frac{1}{2} \sum_{\square} (\nabla \times a)^2 \right\} \tag{49}$$

where U is the (adimensional) Villain potential, λ_0 is the bare screening length and $\sum_{\square}$ runs over all the plaquettes in the array. Finite-size scaling near the Meissner transition is performed on both static quantities (the magnetic field correlation function) [46] and dynamic ones (applying equations (42), (43) to the I–V curve) [47]. The results are consistent with a continuous transition with the same exponent ν as the 3D XY model: $\nu = \nu_{XY} = 2/3$.

In this section we will focus on the effects of temperature (T), disorder (x), the applied magnetic field (f) and anisotropy (η).

Hereafter, by disorder we implicitly mean the bond dilution: x is the fraction of diluted bonds. We stress again that, though dealing with static quantities, the experimental study of superconducting systems often involves dynamic measurements. These can supply extremely

useful information on the static properties of the system (such as the coherence length and critical exponents). Thus at some points we will refer to dynamic behaviour in order to connect theoretical predictions with experimental observations.

5.1. The T-axis ($f = x = 0$)

A resistivity transition occurs at T_c, which belongs to the Berezinskii–Kosterlitz–Thouless transition universality class [48]. T_c separates regimes of low T (there are no free vortices, and zero-current resistance is strictly 0) and high T (free vortices cause a non-zero resistance for any finite current). A trace of this transition is found experimentally in the change of the slope in the I–V curve. The I–V curve is of the type $V \propto I^{a(T)}$. At T_c, $a(T)$ abruptly jumps from $a_{T\to T_c-} = 3$ (below T_c, an applied current, provided that it is high enough, can induce vortex unbinding) to $a_{T\to T_c+} = 1$ [49].

5.2. The x–T plane ($f = 0$) (x is the fraction of diluted bonds)

Along the x-axis, the relevant transition occurs at the percolation threshold (x_p). At this point, the state of the system is characterized by an infinite cluster of superconducting junctions, exhibiting a fractal structure.

For $x > x_p$ there are only isolated finite superconducting clusters, and resistive behaviour is found for any finite current.

For $x < x_p$ a transition to a resistive state may be induced either by an applied current or by increasing the temperature. Though a strict theoretical study of the statics of the system excludes injected current, experimental conditions usually imply working with external currents, and their effects must be taken into consideration in order to understand the results correctly. We will give an overview of the effects of currents. Two questions are in order: Which is the value of the injected current forcing resistive behaviour? Which are the exponents characterizing this current-induced transition?

For every $x < x_p$ the injection of a current above a given value i_c leads to a resistive transition, where the superconducting coherence length is expected to scale as $\xi \sim (i - i_c)^{-\nu_I}$ (we write ν_I so as to make a distinction from the T-induced transition exponent). There is some controversy as regards the value of i_c. A finite i_c could be an artifact of finite-size systems, and would vanish as $L \to \infty$ [50]. However, it has been argued [51] that non-linearities can cause a true non-zero i_c. In this case, i_c is expected to vanish at x_p as $i_c \sim (x_p - x)^v$, where $v = \nu_p(d-1)$ (ν_p being the percolation exponent); in 2D, $v = 4/3$ [51, 52].

We can follow now a reasoning similar to that of section 3: if $i_c \neq 0$ the typical t-scale for relaxation scales as $\tau \sim \xi^z$, and equation (31) suggests again $E \sim (i - i_c)^a$, with

$$a = (z+1)\nu_I. \tag{50}$$

Numerical simulations in 2D suggest $a = 2.4(2)$ and $\nu_I = 1.05(5)$ [53]. These values could be universal critical exponents for $0 < x < x_p$. These results show a satisfactory agreement with the predictions for granular high-T_c materials: $a = t + 1 = 2.3$ (where t is the conductivity exponent of a mixture of resistors and insulators; in 2D, $t = 1.3$) [54]. Different values of a have been proposed: reference [55] concludes that $z = 0.9$, implying a somewhat lower value of a: $a = 1.9$. On the other hand, $a \sim 3$ was reported in [50]. The previous a-values have been obtained for $0 < x < x_p$. Just at x_p, i_c is zero, and the power-law exponent seems to be around 2 [51, 53]. At $x = 0$ (a perfectly ordered array), $v \sim \sqrt{i^2 - 1}$ ($i = I/I_c$). A power series expansion around I_c indicates $v \sim (I - I_c)^{1/2}$, thus giving $a = 1/2$.

What about the effect of temperature? For $x = x_p$ the transition temperature becomes 0, and the power-law exponent of the v–i curve is around 2 [51, 53], a similar value to that

due to the injected current. Thus current and thermal effects are difficult to distinguish. Further analytical and numerical effort is required in order to clarify the critical behaviour of υ. The coherence length diverges as $\xi \sim T^{-\nu_T}$, as happens in the XY model. At $x = x_p$ the linear resistivity in 2D behaves as $\exp(-b/T)$. This $\psi = 0$ value suggests (see equation (35)) that the energy barrier is constant or diverges logarithmically as T decreases. E_b has been calculated to be $E_b = 0.91$ [53], though logarithmic behaviour cannot be completely excluded. The critical exponent ν_T has been calculated through scaling relations, either determining the crossover between the linear and non-linear stretches of the I–V characteristics (equation (39)), or by finding an adequate scaling so that $E/(I\rho_{lin})$ curves obtained for different T merge (equation (37)) [53]. This has been found to be $\nu_T = 1.3(3)$, in accordance with the value predicted by the theory of the correlation length of the diluted XY model at x_p ($\nu = 0.98$–1.03) [56].

5.3. The f–x combined effect

Providing a reasonable description of the processes occurring in real superconductors implies dealing with disorder. Disorder strongly modifies the previously described pictures [84]. For example, for specific values of frustration the order–disorder phase transition is of first order (e.g. $f = 2/5$ in 2D); disorder makes this transition continuous [57].

The combined effect of frustration and disorder provokes the appearance of a vortex glass phase, similar to that described for bulk superconductors: the state of the array is given by a disordered array (no long-range order) of pinned vortices (thus $\rho = 0$).

Dimensionality is a critical parameter for the existence of the vortex glass phase. Theoretically [24] this phase is stable in 3D, not in 2D.

Let us start at 3D. The main predictions of Fisher, Fisher and Huse [24] are: there is a finite-temperature transition to the vortex glass phase ($T_g > 0$); the values of the exponents ν and z are in the ranges $\nu \sim 1$–2, $z \sim 4$–7.

Numerical studies of the I–V curve in the gauge glass and chiral glass models [20, 58] and finite-size scaling of static quantities [59] lead to the following results in the limits of no self-inductance ($\lambda_\perp \to \infty$) and strong screening ($\lambda_\perp \to 0$) (see again figure 3):

- In the case of neglected screening, the transition to the vortex glass phase occurs at a finite temperature ($T = 0.93 \pm 0.05$). The critical exponent ν_T is 1.4 ± 0.3. As far as the value of the dynamic exponent z is concerned, finite-size scaling (equation (43)) gives $z = 3.1(1)$ both for the gauge glass and chiral glass models [20], while Reger *et al* obtain a different value: $z = 4.7 \pm 0.7$ [59].
- In the limit of very strong screening, the critical temperature seems to be 0. The exponent ν, obtained from equations (40) and (41), is 1.05 ± 0.1. As $T_c = 0$, the relevant dynamic exponent is ψ, with a value $\psi \approx 0$, indicating that energy barriers between neighbouring minima remain constant or diverge logarithmically as $T \to 0$.

The first direct evidence of a low-temperature vortex glass phase in a disordered superconductor was obtained for YBCO thin films [60]. Since then, numerous experimental results on YBCO films have confirmed the theoretical predictions [61–63]: for thick enough films (thickness $t \geqslant 1000$ Å), the values obtained for ν and z are, respectively, in the ranges 1.1–1.9 and 4.4–6. Recent experiments on cubic (K, Ba)BiO_3 superconductors [42] give $\nu = 1 \pm 0.2$, while $z = 5.0 \pm 0.6$, both exponents remaining constant along the f–T vortex glass transition line.

In 2D systems the main predictions of the FFH theory for the vortex glass phase are: the transition occurs at $T_g = 0$, $\nu \sim 2$; and $\rho_{lin} \propto \exp(-(T/T_0)^p)$ with $p = 1 + \Psi\nu \geqslant 1$ (from equation (35)) [24].

Numerical simulations in 2D using both the gauge glass and a random-pinning Hamiltonian (equation (26)) show, in accordance with the experiments, that $T_g = 0$ and $\nu \simeq 2$ [23]. The linear resistivity is calculated to scale as $T\rho_{lin} \sim \exp(-a/T)$ (thus $p = 1$).

Recent simulations with the 2D chiral glass model [21], in accordance with the gauge glass model, show that the scaling analysis of the I–V curve is consistent with a phase transition at $T = 0$. At this limit, ρ_{lin} has an Arrhenius behaviour: $\ln \rho_{lin} \sim -a/T$. The correlation length diverges as $\xi \sim T^{-\nu_T}$, with $\nu_T = 1.1(2)$, as determined by using both equations (37) and (39). Thus 2D chiral glass and gauge glass are in different universality classes. A deeper examination of the model throws some light on the nature of the transition. Unlike the case for the gauge glass model, and reflecting the fact that there is an extra reflection symmetry, the zero-temperature transition of the 2D chiral glass is characterized by two correlation lengths: ξ_c, corresponding to chiral glass order, and ξ_s, which indicates the phase correlation length. They have different critical exponents: $\nu_c \sim 2$ (just as in the gauge glass model) and $\nu_s \sim 1$. Thus resistivity measurements probe the phase correlation length.

What about experiments? A 2D vortex glass transition was found in ultrathin (one unit cell thick) YBCO films [62, 64]. The current at which non-linear resistance has its onset was measured to scale with temperature as $I_{nl} \sim T^{3\pm0.3}$, in coincidence with the theoretical prediction $\nu = 2$. The scaling expression (37) was verified provided that ρ_{lin} behaves as $\rho_{lin} \sim \exp(-a/T^p)$, with $p \simeq 0.6$. Such a value of p (versus the prediction $p = 1 + \Psi\nu \geqslant 1$) is hard to explain in terms of a classical description (thermal activation of correlated bundles of vortices), and rather suggests that quantum effects (e.g. quantum tunnelling of vortices through energy barriers) are relevant [65]. Recently, experimental results fully consistent with the predictions $T_g = 0$, $\nu = 2$ and $p > 1$ have been obtained for highly anisotropic $Tl_2Ba_2CaCu_2O_8$ thin films subjected to high magnetic fields (so as to guarantee full penetration in the sample) [66].

What about intermediate-thickness superconductors? In reference [67] the vortex glass transition in $YBa_2Cu_3O_{7-\delta}$ films whose thickness ranges from 18 up to 1000 nm is studied. All of them show a clear scaling collapse in the $E/(J|t|^{\nu(z+2-d)})$ versus $J/(T|t|^{\nu(d-1)})$ curves (see equations (36) and (38)), giving clear evidence of a second-order transition. The results for the thicker films are consistent with the 3D theoretical predictions. T_g is seen to decrease with the thickness, but for the thinner films ($t \sim$ 18–75 nm) the behaviour departs from the predictions. The authors of [67] postulate the need for an anisotropic 3D vortex glass theory in order to explain the physics of films with a thickness intermediate between those for the 3D bulk and real 2D systems. An anisotropic scaling is proposed, with two different correlation lengths ($\xi_\perp$ and $\xi_\parallel$, respectively perpendicular and parallel to the c-plane), characterized by different static exponents $\nu_\perp$ and $\nu_\parallel$: $\nu_\parallel = \alpha\nu_\perp$ with $\alpha < 1$.

We turn now to the model obtained by bond dilution of equation (1). Here the level of disorder is tunable by selecting the fraction of diluted bonds (x). As x varies, different regions of the f–x–T phase diagram are explored.

At zero dilution ($x = 0$) the ground state is described by a periodic pinned vortex lattice whose cell array is in general $q \times q$. Two transitions compete as T varies. On the one hand, the Kosterlitz–Thouless mechanism of vortex unbinding leads to the superconducting transition at T_S. Another relevant temperature is T_{VL}, corresponding to the melting of the vortex lattice due to domain wall excitations. For $f = 0, 1/2$ and other low rational values of f, the two transitions are very close: $T_{VL} \geqslant T_S$.

In the absence of an external field ($f = 0$), Hamiltonian (1) reproduces the diluted XY

model, which is known to be a superconductor for $x < x_p$ [56].

If frustration is present, there is a threshold x_{VL} for lattice ordering below x_p [68]. It has been recently argued [22] that disorder leads to the separation of the two transitions:

- The superconducting phase persists for $x < x_s(f)$. At $x_s(f)$, T_c becomes 0.
- Within a range $x_s(f) < x < x_{VL}(f)$, vortex lattice ordering persists.
- Above $x_{VL}(f)$, and before the percolation threshold is reached ($x_{VL}(f) < x < x_p(f)$), there is a region characterized by the lack of long-range order, which is a candidate for accommodating a vortex glass phase. In 2D a vortex glass occurs in this region only on the $T = 0$ line.

Let us consider rational values of the frustration $f = p/q$. x_{VL} corresponds roughly to the percolation threshold of a $q \times q$ lattice, which is reached far below the single-bond percolation threshold ($x_{VL} < x_p$). As vortex lattice disordering provokes the suppression of phase coherence, x_{VL} is an upper limit for superconductivity ($x_s \leqslant x_{VL}$). The picture is completed by considering the dependence of x_{VL} on f. For low-order rational frustration, if $f' < f$, this implies that $q' > q$; thus the unit cell corresponding to f' is greater than that corresponding to f, and $x_{VL}(f')$ occurs before $x_{VL}(f)$. Consequently, one expects $x_{VL}(f') < x_{VL}(f)$. A sketch of the different phases is shown in figure 8.

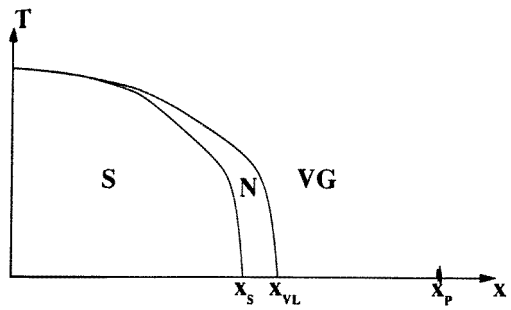

Figure 8. A schematic phase diagram of a diluted 2D JJA. S, N and VG stand for the superconducting, normal (ordered vortex lattice) and vortex glass phases. We stress that, in 2D, the vortex glass phase exists only at $T = 0$. Courtesy of Benakli, Granato, Shenoy and Gabay [22].

Numerical work verifies this scheme for a bond-diluted, triangular JJA at $f = 1/2$ and $T = 0$ [22]. The stability of the ordered phases is studied following the domain renormalization group method [69] through a recently developed optimized algorithm [70]. First of all, the ground state is determined for a realization of disorder in a system of a given length L. Then a change is imposed on the boundary conditions, and the energy of the resulting configuration is related to that of the initial ground state:

- On imposing antiperiodic boundary conditions, the energy difference $\Delta E_{ap} = E_a - E_p$ is a measure of the phase coherence (and thus indicates the existence of a superconducting state): it is finite in a phase-coherent state, 0 otherwise.
- On imposing periodic boundary conditions, the energy difference $\Delta E_{rp} = E_r - E_p$ is a measure of the energy cost for a domain wall in the vortex lattice. It gives an indication of the vortex lattice order.

ΔE_{ap} and ΔE_{rp} should be averaged over for different realizations of the disorder for each x-value. The averaged results are referred to as $[\Delta E_{ap}](x)$ and $[\Delta E_{rp}](x)$. $[\Delta E](x)$ constant or increasing with L implies the stability of the ground state. For small values of x, $[\Delta E](x)$

increases with the size of the array: long-range coherence (vortex lattice order) exists. For large values of x, $[\Delta E](x)$ decreases with the size of the array, giving evidence of a lack of long-range coherence (vortex lattice order). The change in the behaviour as L increases gives the value of x_s (x_{VL}). For $f = 1/2$, $T = 0$, x_s is measured to be smaller than x_{VL}. Stability analysis at $x_{VL} < x < x_p$ shows that the vortex glass phase occurs only at $T = 0$.

An intriguing question is that of under which circumstances (array geometry, level and kind of disorder) disorder may endanger even the existence of an ordered vortex phase. For $f = 0$, an ordered phase survives for low enough disorder [71]: for a disorder level $\sigma < \sigma_c$ this phase exists for $T < T_c(\sigma)$ (here σ stands for positional disorder). For $f = 1/2$ (a fully frustrated Josephson junction array) the system exhibits two symmetries: a continuous one (U(1)) and a discrete one (Z_2), related respectively to a *'KT-like' order* and an *'Ising-like' order*. The persistence of an ordered phase in the presence of positional disorder in a square array has been studied for $f = 1/2$ [72]; it is claimed that the ordered phase persists for weak disorder. However, recently Gupta and Teitel [73] arrived at the opposite conclusion for $f = 1/2$ on the basis of the analogy with the random-field Ising model. Their conclusion is that, in the thermodynamic limit (the size of the system tending to infinity), the critical disorder is $\sigma_c = 0$: any amount of finite disorder destroys the *'Ising-like' order*; thus the ground-state vortex lattice would always be disordered for any non-zero value of σ. The non-zero σ_c obtained in the previous reference ([72]) would be a finite-size effect: the correlation length, though finite, would be longer than the system under simulation, leading to the illusion of a diverging ξ, and thus of a disorder–order second-order transition.

5.4. The f–T plane: glassiness in the absence of disorder

A relevant problem is that of the superconducting critical line $T_c(f)$. It has been suggested (by Teitel and Jayaprakash, in reference [29]) that the superconducting temperature is a very discontinuous function of f: $T_c(f) \leqslant 1/q$, with the result that $T_c \to 0$ for irrational values of f.

The Hamiltonian (1) reduces, if self-inductance effects are negligible, to the uniformly frustrated XY model. Its low-temperature state is characterized by two kinds of broken symmetry: the U(1) symmetry (*'KT-like order'*), associated with superconducting phase coherence, plus a discrete symmetry. Basically, for rational values of the frustration $f = p/q$ the discrete symmetry is known to be Z_q. This added discrete symmetry influences the nature of the order–disorder phase transition. As q has a singular dependence on f, the nature of the phase transition varies with f in a rather complicated way. For $f = 1/2$, the discrete symmetry is Z_2: interchanging the vortex and antivortex leaves the ground state invariant. For $f = 1/3$, for example, the discrete symmetry group is $Z_2 \times Z_3$ [74]. The transition to the ordered phase is strongly influenced by the energy cost of domain walls [57]: for $f = 1/3$ a binding of two walls is not energetically favourable, and the transition is continuous; however, for $f = 2/5$ the lowest-energy walls tend to bind. When this binding is taken into account, the free energy of the system at the critical temperature becomes discontinuous; thus the transition is first order.

An intriguing problem is that of the appearance of glassy behaviour for irrational f-values. Unlike the case in previous subsection, where a vortex glass state resulted from the combined effect of disorder and frustration, here we deal with perfectly ordered arrays, where the Hamiltonian exhibits no intrinsic disorder. These glassy systems can be referred to as *structural glasses*, and their glass transition is still far from being satisfactorily understood [75]. Josephson arrays arise, again, as experimental systems especially appropriate to the study of complex condensed matter problems. It was claimed on the basis of Monte Carlo simulations

(see Halsey, in reference [29]) that, in the limit of an irrational $f^* = (3 - \sqrt{5})/2$, an ordered 2D array undergoes a glass transition to a superconducting disordered vortex state at a finite temperature $T_g \neq 0$. This result was partially supported by experiments on superconducting wire networks at f^* [76]. However, this result is not directly applicable to a granular JJA: each wire is connected to many other 'first neighbours' (any horizontal wire is nearest neighbour to any vertical one, and vice versa). The transition undergone by this system would correspond to that of a higher-dimension JJA (we stress that dimensionality is crucial to the existence of a non-zero T_g).

On the other hand, numerical simulations of the dynamics of an ordered 2D resistively shunted junction array showed a scaling relation (equation (37)) which suggested a zero-temperature glass transition [77]. The critical exponent $\nu = 0.9 \pm 0.2$ was found to be different to that obtained for systems with disorder ($\nu \sim 2$), reflecting the different nature of the ground states of ordered and disordered arrays.

New arguments have been added to the $T_g(f^*) = 0$ (dynamic) versus $T_g(f^*) \neq 0$ (Monte Carlo) controversy [78]. In reference [78], a Monte Carlo simulation of the Coulomb gas dual to the uniformly frustrated 2D JJA is performed. At a given temperature T_c (coinciding with Halsey's T_g) a first-order transition to an ordered vortex structure, consisting in successive diagonals which are completely filled, completely empty and partially filled with vortices, occurs. In the successive Monte Carlo runs, vortices are free to move along the partially filled diagonals (thus leading to phase incoherence) down to a pinning temperature $T_p(f)$. T_c is slightly dependent on f. The characterization of the $T_c > T > T_p(f)$ region as a disordered, glassy vortex state in [29] was an artifact, induced by the specific algorithm used.

5.5. The effect of anisotropy

A parameter frequently used when modelling 3D superconductors is anisotropy. Some granular high-T_c materials can be described as a series of stacked planar arrays (e.g., $Bi_2Sr_2CaCu_2O$ [79]). The critical currents in the direction perpendicular to the planes are lower than those in the in-plane directions. A phenomenological free-energy function F, inspired by simulations on 3D Josephson arrays, was proposed in reference [80]. It explains how the first-order superconductivity transition smooths, becoming continuous due to disorder. The anisotropy (η) was defined by $i_{C\perp} = i_0/\eta^2$, where $i_{C\perp}$ is the critical current in the direction perpendicular to the planes (resistances are increased by the same value). The in-plane critical currents are of the order of $i_{C\parallel} \sim i_0$. Disorder (D) is modelled through random distribution of the critical current values. The resulting phase diagram is shown in figure 9. For $\eta = \infty$, different planes are decoupled, so the system reduces to a set of independent 2D arrays. For $\eta = 0$, due to the extremely strong inter-plane coupling, vortices are rigid lines, and the system reduces to an equivalent 2D one. The superconducting transition in 2D is second order. For intermediate

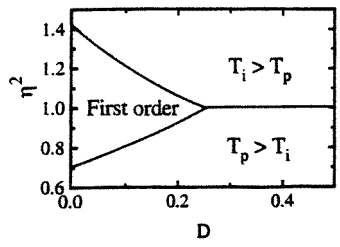

Figure 9. The disorder–anisotropy phase diagram. Courtesy of Jagla and Balseiro [80].

η-values the system is truly 3D. The authors of [80] postulate the existence of two different continuous transitions, characterized by the depinning of independent vortices (occurring at T_i) and the percolation transition (at T_p, whose order parameter is the probability of having a vortex path starting from one lateral side of the array and finishing on the other). For high enough disorder, two regions can be distinguished:

- For small η, in-plane and inter-plane coherence are lost, respectively, at T_i and T_p ($T_i < T_p$) (the loss of phase coherence, and thus that of superconductivity, is detected by there being non-zero resistivity and, equivalently, the helicity modulus going to zero).
- For large η, in-plane and inter-plane coherence are lost; the vortex structure percolates at $T_p < T_i$ (in-plane and inter-plane coherence are lost at T_i).

For low D, within an intermediate η-range the two continuous transitions coincide, merging into a first-order one. As regards the external field f, scaling arguments are used to reduce the 3D parameter space (D, η, f) to a 2D space, whose variables are $a = \eta^2 f$ and $b = D^2 f$. Thus, the phase diagram for any value of f can be referred to that for a reference f^*: the properties of the system at (D_1, η_1, f_1) ($f_1 = \alpha f$) are the same as those at ($\sqrt{\alpha} D$, $\sqrt{\alpha}\eta$, f^*).

5.6. Large junctions

Another question deserving mention is that of 2D (large-area) Josephson junctions. It arises when the junction dimensions are larger than the magnetic field penetration depth ($L > \lambda$), as happens in trilayer junctions like $YBa_2Cu_3O_x/YBa_2Cu_3O_x/YBa_2Cu_3O_x$ [81] and $Bi_2Sr_2CaCu_2O_8/Bi_2Sr_2Ca_7Cu_8O_{20}/Bi_2Sr_2CaCu_2O_8$ [82]. In this case, the junction state is given by a phase ϕ which varies continuously along and across the junction. A phase diagram of a 2D junction has been proposed in reference [83], as a function of temperature and disorder (here disorder is due to the random magnetic fields arising from quenched flux loops trapped in the bulk superconductor). The relevant order parameters are $z = \langle\cos(\phi)\rangle$ (measuring long-range order in the phase) and a glass order parameter Δ (the glassy state is characterized by a slow relaxation). The replica-symmetry-breaking method was applied to study the free energy of the system, and four different phases were found:

- At high temperatures thermal fluctuations dominate, and we have a disordered ($z = 0$, $\Delta = 0$) phase.
- In the presence of strong disorder, lowering the temperature leads to a glass phase ($z = 0$, $\Delta \neq 0$)
- In the presence of weak disorder, as temperature diminishes first a Josephson phase occurs ($z \neq 0$, $\Delta = 0$).
- At even lower temperature (weak disorder) a first-order transition leads to a new phase where Josephson order and glassy behaviour coexist ($z \neq 0$, $\Delta \neq 0$).

6. Conclusions

Josephson junction arrays have proved to be very useful as available model systems for providing an understanding of the properties of high-T_c superconductors and, in general, for exploring the physics of complex non-linear systems.

In fact, JJAs are suitable systems for exhibiting glassy behaviour, which may be induced either by intrinsic disorder (positional disorder, critical current dispersion) or by external perturbation (such as a magnetic field). For high-T_c materials, the strong effects of thermal fluctuations and defects render study extremely difficult. The possibility of both simulating and fabricating arrays where the nature and the amount of disorder are fixed with an acceptable

degree of precision, and the sophisticated experimental facilities available nowadays, allow a detailed study of arrays under perfectly controlled conditions. Results can be extrapolated to granular high-T_c superconductors, where an intrinsic Josephson effect is present.

The phase diagram of a JJA as a function of temperature (T), disorder (x) and the applied magnetic field (f) is commented on in the light of recent results. The main benchmarks are as follows:

- *Along the f-axis ($T = x = 0$)*, we study the ground states, and the stability of the equilibrium vortex configurations. In 2D arrays, the vortex density of the ground state (the average number of vortices per plaquette) is $w(f) = f$. The vortex configuration results from competition between the natural tendency of vortices to arrange in triangular lattices (as happens in superconducting films) and the need to accommodate to the periodic potential of the array (with a minimum at each plaquette). In a ladder, however, $w(f)$ climbs up a Devil's staircase, which persists for any value of the magnetic penetration depth $\lambda_\perp$.
- *Along the T-axis*, the relevant temperature is that characterizing the Kosterlitz–Thouless transition. T_{KT} separates the phases with no free vortices and uncoupled vortices.
- *Along the x-axis*, the relevant parameter is the percolation threshold (x_p), where the system has an infinite cluster of superconducting junctions which exhibit a fractal structure.
- *In the x–T plane*, for each $x < x_p$ there is a critical temperature which ranges from T_{KT} for $x = 0$ down to $T_c = 0$ at $x = x_p$. This transition leaves its mark in the I–V curve, and can be identified under experimental conditions. Care must be taken, however, because the effect of the injected current is also relevant: current-induced transition is characterized by a value of ν similar to that due to thermal fluctuations. Moreover, it is not clear whether i_c (the current leading to resistive transition) is different from zero; if $i_c = 0$, current-induced effects would appear unavoidably.
- *The f–x combined effect* leads to the appearance of the vortex glass phase, characterized by the pinning of vortices to randomly placed lattice defects. Due to vortex pinning, the resistivity is zero. Moreover, as the positions of the defects are random, there is no long-range order in the vortex lattice. The critical temperature for the transition to the vortex glass phase is finite for 3D and zero for 2D, as seen both in theoretical models and in experiments. For superconductors with an intermediate thickness, an anisotropic scaling is proposed. The appearing of the vortex phase depends on the value of the frustration, and also on the geometry of the array.
- *In the f–T plane*, both the nature and the critical temperature of the transition to the superconducting phase show a rather involved dependence on f. The critical temperature ($T_c(f) \leqslant 1/q$) is a highly discontinuous function of the frustration, with value zero for irrational f. The nature (first or second order) of the transition is strongly influenced by the discrete Z_q symmetry associated with the frustrated XY model with $f = p/q$; variation of f leads the discrete symmetry group to vary in a complicated way.

  We also consider the problem of *'structural glasses'*: transition to a disordered state is found in perfectly ordered arrays. Dimensionality is again a critical feature (in 2D the temperature for the transition to the glassy phase seems to be $T_g = 0$).
- We also consider the effects of the *anisotropy*, both in the nature of the ground states and in the general disorder–temperature–anisotropy phase diagram. According to the anisotropy level, a material is equivalent to a stack of independent planar systems ($\eta \gg 1$), to an effective 2D one ($\eta \ll 1$), or to one showing a truly 3D behaviour for intermediate η. Thus anisotropy affects the effective dimensionality of the system and thus the order of its transition to the disordered phase.

References

[1] As an introduction to the subject of JJAs, see
Giovannella C and Lambert C (ed) 1997 *Superconductivity in Networks and Mesoscopic Systems* (New York: AIP)
while as a reference book on the Josephson physics, see
Likharev K K 1986 *Dynamics in Josephson Junctions and Circuits* (New York: Gordon and Breach)
Barone A and Paterno G 1982 *Physics and Application of the Josephson Effect* (New York: Wiley)

[2] For a recent review on the state of the art, see
Giovannella C and Tinkham M (ed) 1995 *Macroscopic Quantum Phenomena and Coherence in Superconducting Networks* (Singapore: World Scientific)
Cerdeira H A and Shenoy S R (ed) 1996 *Physica* B **222** 253

[3] Müller K A Takashige M and Bednorz J G 1987 *Phys. Rev. Lett.* **58** 1143

[4] See, for example,
Giovannella C, Chappert C, Beauvillain P and Collin G 1987 *Int. J. Mod. Phys.* B **1** 1011
Giovannella C 1989 *Phys. Status Solidi* **154** 273
Tinkham M 1988 *Phys. Rev. Lett.* **61** 1658
Yeshurun Y and Malozemoff A P 1988 *Phys. Rev. Lett.* **60** 2202

[5] Kleiner R, Müller P, Kohlstedt H, Pedersen N F and Sakai S 1994 *Phys. Rev.* B **50** 3942
Kleiner R and Müller P 1994 *Phys. Rev.* B **42** 1327

[6] Tsvetkov A A, van der Marel D, Moler K A, Kirtley J R, de Boer J L, Meetsma A, Ren Z F, Koleshnikov N, Dulic D, Damascelli A, Grueninger M, Schuetzmann J, van der Eb J W, Somal H S and Wang J H 1998 *Nature* **395** 360
Il'ichev E, Zakosarenko V, Ijsselsteijn R P J, Schultze V, Meyer H-G, Hoening H E, Hilgenkamp H and Mannhart J 1998 *Phys. Rev. Lett.* **81** 894
Habib Y M, Lehner C J, Oates D E, Vale L R, Ono R H, Dresselhaus G and Dresselhaus M S 1998 *Phys. Rev.* B **57** 13 833

[7] See, for recent examples,
Castro Neto A H and Guinea F 1998 *Phys. Rev. Lett.* **80** 4040
Hu X and Tachiki M *Phys. Rev. Lett.* **80** 4044

[8] Ciria J C and Giovannella C 1998 *J. Phys.: Condens. Matter* **10** 1453
Ciria J C and Giovannella C 1998 *Lectures on Superconductivity in Networks and Mesoscopic Systems* ed C Giovannella and C Lambert (New York: AIP) p 70

[9] Majhofer A, Wolf T and Dieterich W 1991 *Phys. Rev.* B **44** 9634
Dominguez D and José J V 1994 *Int. J. Mod. Phys.* B **8** 3749

[10] Phillips J R, van der Zant H S J, White J and Orlando T P 1993 *Phys. Rev.* B **47** 5219

[11] Demler E, Berlinsky A J, Kallin C, Arnold G B and Beasley M R 1998 *Phys. Rev. Lett.* **80** 2917
den Hertog B C, Berlinsky A J and Kallin C 1998 *Preprint* cond-mat/9811133

[12] Chen D X, Moreno J J and Hernando A 1997 *Phys. Rev.* B **56** 2364

[13] van der Zant H J S, Rijken H A and Mooij J E 1983 *J. Low Temp. Phys.* **27** 150

[14] Ciria J C and Giovannella C 1997 *J. Phys.: Condens. Matter* **9** 2571

[15] José J V, Kadanoff L P, Kirpatrick S and Nelson D R 1977 *Phys. Rev.* B **16** 1217

[16] Mazo J J and Ciria J C 1997 *Phys. Rev.* B **68** 16 068

[17] Villain J 1975 *J. Physique* **36** 581

[18] Vallat A and Beck H 1994 *Phys. Rev.* B **50** 4015

[19] Zachar O 1998 *Preprint* cond-mat/9810321

[20] Wengel C and Young P 1997 *Phys. Rev.* B **56** 5918

[21] Granato E 1998 *Phys. Rev.* B **58** 11 161

[22] Benakli M, Granato E, Shenoy S R and Gabay M 1998 *Phys. Rev.* B **57** 10 314

[23] Hyman R A, Wallin M, Fisher M P A, Girvin S M and Young A P 1995 *Phys. Rev.* B **51** 15 304

[24] Fisher D S, Fisher M P A and Huse D A 1991 *Phys. Rev.* B **43** 130

[25] Hohenberg P C and Halperin B I 1977 *Rev. Mod. Phys.* **49** 435
Privman V (ed) 1990 *Finite Size Scaling and Numerical Simulations of Statistical Systems* (Singapore: World Scientific)

[26] Tinkham M 1996 *Introduction to Superconductivity* 2nd edn (New York: McGraw-Hill)

[27] Halperin B I and Nelson D R 1979 *J. Low Temp. Phys.* **36** 1165
Doniach S and Huberman B A 1979 *Phys. Rev. Lett.* **42** 1169
Fisher D S 1980 *Phys. Rev.* B **22** 1190

[28] Minnhagen P 1987 *Rev. Mod. Phys.* **59** 1001
[29] Teitel S and Jayaprakash C 1983 *Phys. Rev. Lett.* **51** 1999
Halsey T C 1985 *Phys. Rev. Lett.* **55** 1018
Kolahchi M R and Straley J P 1991 *Phys. Rev.* B **43** 7651
[30] Straley J P and Barnett G M 1993 *Phys. Rev.* B **48** 3309
[31] Franz M and Teitel S 1995 *Phys. Rev.* B **51** 6551
[32] Kolahchi M R 1997 *Phys. Rev.* B **56** 95
[33] Mazo J J, Falo F and Floria L M 1995 *Phys. Rev.* B **52** 10 433
[34] An extensive list of references on the Frenkel–Kontorova model can be found in
Floria L M and Mazo J J 1996 *Adv. Phys.* **45** 505
[35] Griffiths R B and Chou W 1986 *Phys. Rev. Lett.* **56** 1929
Sasaki K and Griffiths R B 1988 *J. Stat. Phys.* **53** 1031
[36] Denniston C and Tang C 1995 *Phys. Rev. Lett.* **75** 3930
[37] Barahona M and Strogatz S H 1998 *Phys. Rev.* B **58** 5215
[38] Nuvoli A, Giovannella C and Ciria J C 1997 unpublished
[39] Barahona M and Watanabe S 1998 *Phys. Rev.* B **57** 10 893
[40] Barahona M, Strogatz S H and Orlando T P 1998 *Phys. Rev.* B **57** 1181
[41] Deak J, Hou L, Metcalf P and McElfresh M 1995 *Phys. Rev.* B **51** 705
[42] Klein T, Conde-Gallardo A, Marcus J, Escribe-Filippini C, Samuely P, Szabó P and Jansen A G M 1998 *Phys. Rev.* B **58** 12 411
[43] Dominguez D, Jensen N G and Bishop A R 1995 *Phys. Rev. Lett.* **75** 4670
[44] Jagla E A and Balseiro C A 1996 *Phys. Rev. Lett* **77** 1588
[45] Dasgupta C and Halperin B I 1981 *Phys. Rev. Lett.* **47** 1556
[46] Olsson P and Teitel S 1998 *Phys. Rev. Lett.* **80** 1964
[47] Lidmar J, Wallin M, Wengel C, Girvin S M and Young A P 1998 *Phys. Rev.* B **58** 2827
[48] Kosterlitz J M and Thouless D J 1972 *J. Phys C: Solid State Phys.* **5** L124
Kosterlitz J M and Thouless D J 1973 *J. Phys C: Solid State Phys.* **6** L1181
Berezinskii V L 1972 *Zh. Eksp. Teor. Fiz.* 1972 **61** 61 (Engl. Transl. 1972 *Sov. Phys.–JETP* **34** 610)
[49] Lobb C J, Abraham D W and Tinkham M 1983 *Phys. Rev.* B **27** 150
[50] Leath P L and Xia W 1991 *Phys. Rev.* B **44** 9619
[51] Lee K H and Stroud D 1992 *Phys. Rev.* B **45** 1417
[52] Lobb C J, Hui P M and Stroud D 1987 *Phys. Rev.* B **36** 1956
[53] Granato E and Dominguez D 1997 *Phys. Rev.* B **56** 14 671
[54] Prester M 1996 *Phys. Rev.* B **54** 606
[55] Tiesinga P H E, Hagenaars T J, van Himbergen J E and José J V 1997 *Phys. Rev. Lett.* **78** 519
[56] Stauffer D and Aharony A A 1992 *Introduction to Percolation Theory* (London: Taylor and Francis)
[57] Denniston C and Tang C 1997 *Phys. Rev. Lett.* **79** 451
Denniston C and Tang C 1998 *Phys. Rev.* B **58** 6591
[58] Kawamura H and Li M S 1996 *Phys. Rev.* B **54** 619
Kawamura H and Li M S 1997 *Phys. Rev. Lett.* **18** 1556
[59] Reger J D, Tokuyasu T A, Young A P and Fisher M P A 1991 *Phys. Rev.* B **44** 7147
[60] Dekker C, Eidelloth W and Koch R H 1992 *Phys. Rev. Lett.* **68** 3347
[61] Olson H K, Koch R H, Eidelloth W and Robertazzi R P 1991 *Phys. Rev. Lett.* **66** 2661
Roberts J M, Brown B, Hermann B A and Tate J 1994 *Phys. Rev.* B **49** 6890
Hou L, Deak J, Metcalf P and McElfresh M 1997 *Phys. Rev.* B **55** 11 806
[62] Wöltgens P J M, Dekker C, Koch R H, Hussey B W and Gupta A 1995 *Phys. Rev.* B **52** 4536
[63] Joshi R J, Hallock R B and Taylor J A 1997 *Phys. Rev.* B **55** 9107
[64] Dekker C, Wöltgens P J M, Koch R H, Hussey B W and Gupta A 1992 *Phys. Rev. Lett.* **69** 2717
[65] Fisher M P A, Tokuyasu A and Young A P 1991 *Phys. Rev. Lett.* **66** 2931
[66] Wen H, Radovan H A, Kamm F-M, Ziemann P, Yan S L, Fang L and Si M S 1998 *Phys. Rev. Lett.* **80** 3859
[67] Sawa A, Yamasaki H, Mawatari Y, Obara H, Umeda M and Kosaka S 1998 *Phys. Rev.* B **58** 2868
[68] Giamarchi T and Le Doussal P 1994 *Phys. Rev. Lett.* **72** 1530
[69] Cieplak M and Banavar J R 1984 *Phys. Rev.* B **29** 469
McMillan W L 1985 *Phys. Rev.* B **31** 342
[70] Maucourt J and Grempel D R 1998 *Phys. Rev. Lett.* **80** 770
[71] Maucourt J and Grempel D R 1997 *Phys. Rev.* B **56** 2572
Kosterlitz J M and Simkin M 1997 *Phys. Rev. Lett.* **79** 1098
[72] Cataudella V 1998 *Europhys. Lett.* **44** 478

[73] Gupta P and Teitel S 1998 *Preprint* cond-mat/9812157
[74] Grest B 1989 *Phys. Rev.* B **39** 9267
Lee S and Kee K-C 1995 *Phys. Rev.* B **52** 6706
[75] Rubi M and Pérez-Vicente C (ed) 1997 *Complex Behavior of Glassy Systems* (New York: Springer)
[76] Yu F, Israeloff N E, Goldman A M and Bojko R 1992 *Phys. Rev. Lett.* **68** 2535
[77] Granato E 1996 *Phys. Rev.* B **54** 9655
[78] Gupta P, Teitel S and Gingrass J P 1998 *Phys. Rev. Lett.* **80** 105
[79] Cruz F, Rodriguez E, Pastoriza H, Arriberi A and Goffmann M F 1994 *Physica* B **197** 596
[80] Jagla E A and Balseiro C A 1997 *Phys. Rev.* B **55** 3192
[81] Štrbik V, Chromik Š, Baňačka Š and Karlovský K 1996 *Czech. J. Phys.* **46** 1313
Cucolo A M, Di Leo R, Nigro A, Romano P, Bobba F, Bacca E and Prieto P 1996 *Phys. Rev. Lett.* **76**
[82] Virshup G F, Klausmeier-Brown M E, Bozovic I and Eckstein J N 1992 *Appl. Phys. Lett.* **60** 2288
[83] Horovitz B and Golub A 1997 *Phys. Rev.* B **55** 14 499
[84] Giannelli A, Giovannella C and Bernaschi M 1993 *Europhys. Lett.* **22** 29
Giannelli A, Giovannella C and Bernaschi M 1994 *Physica* B **194–196** 1695